geosciences

MDPI

Article

Nb-Ta-Sn Oxides from Lithium-Beryllium-Tantalum Pegmatite Deposits of the Kolmozero–Voronja Belt, NW Russia: Implications for Tracing Ore-Forming Processes and Mineralization Signatures

Dmitry Zozulya [1,*], Lyudmila N. Morozova [1,2], Kåre Kullerud [3] and Ayya Bazai [1]

[1] Geological Institute of the Kola Science Centre of the Russian Academy of Sciences, 14 Fersman St., 184209 Apatity, Russia
[2] All-Russian Scientific-Research Institute of Mineral Resources Named after N.M. Fedorovsky, 31 Staromonetny ln, 119017 Moscow, Russia
[3] Norwegian Mining Museum, Hyttegata 3, 3616 Kongsberg, Norway; kk@bvm.no
* Correspondence: zozulya@geoksc.apatity.ru

Abstract: In this paper we present textural and compositional data for columbite group minerals (CGMs) and associated Nb-Ta-Sn oxides from lithium-beryllium-tantalum pegmatite deposits of the Kolmozero–Voronja belt, NW Russia, with the aim of deciphering these characteristics for minerals from deposits with different mineral signatures and lithium ore grade. Minerals from four deposits, including two of world-class (Kolmozero and Polmostundra), are examined. The main controlling factors for CGM compositional ranges are the diversity and rate of magmatic fractionation, hydrothermal overprint and mineral paragenesis, following the specific geochemical signature of the different pegmatite deposits. CGM from Kolmozero include several mineral species (columbite-(Fe), columbite-(Mn), tantalite-(Fe), and tantalite-(Mn)), showing large compositional variations, mainly controlled by Nb-Ta fractionation (Ta/(Ta + Nb) = 0.16–0.70; Mn/(Mn + Fe) = 0.45–0.63). Textural patterns are various (oscillatory, homogeneous, and patchy); spongy domains and overgrowing Ta-rich rims are also observed somewhere. This indicates the involvement of numerous magmatic and hydrothermal processes. The Polmostundra CGMs are represented by columbite-(Fe) with Ta/(Ta + Nb), ranging from 0.05 to 0.39; some crystals are homogenous, and others present normal, oscillatory, mottled and reverse-zoning patterns. The Okhmylk CGMs are irregular normal, patchy and homogeneous columbite-(Fe) and columbite-(Mn), with Ta/(Ta + Nb) = 0.09–0.24 and Mn/(Mn + Fe) = 0.29–0.92, indicating the suppressed magmatic fractionation and iron drop due to precipitation of Fe minerals. Columbite-(Fe) and columbite-(Mn) from the Be-Ta Shongui deposit are less evolved, with Ta/(Ta + Nb) = 0.07–0.23 and Mn/(Mn + Fe) = 0.31–0.55. The minerals are characterized by progressive normal, oscillatory, homogeneous and irregular reverse patterns. Associated pyrochlore minerals occur both as early magmatic (Kolmozero) and late hydrothermal (Polmostundra, Okhmylk). Cassiterite is found only in the Okhmylk dykes, and is apparently of hydrothermal origin. CGM from Li pegmatites have impurities of Ti (0.01–0.05 apfu) and W (up to 0.02 apfu), whereas CGM from Be pegmatites contains elevated Ti (up to 0.09 apfu). The mineral system analysis presented here is relevant for exploration.

Keywords: columbite group minerals; pyrochlore; cassiterite; pegmatite; lithium; beryllium; NW Russia

check for updates

Citation: Zozulya, D.; Morozova, L.N.; Kullerud, K.; Bazai, A. Nb-Ta-Sn Oxides from Lithium-Beryllium-Tantalum Pegmatite Deposits of the Kolmozero–Voronja Belt, NW Russia: Implications for Tracing Ore-Forming Processes and Mineralization Signatures. *Geosciences* **2024**, *14*, 9. https://doi.org/10.3390/geosciences14010009

Academic Editors: Jaime Cuevas Rodríguez and Jesus Martinez-Frias

Received: 1 November 2023
Revised: 17 December 2023
Accepted: 22 December 2023
Published: 24 December 2023

Copyright: © 2023 by the authors. Licensee MDPI, Basel, Switzerland. This article is an open access article distributed under the terms and conditions of the Creative Commons Attribution (CC BY) license (https://creativecommons.org/licenses/by/4.0/).

1. Introduction

Columbite-group minerals (CGM) with the ideal formula AB_2O_6 (A = Mn, Fe; B = Nb, Ta) are important accessory minerals in granitic pegmatites, and constitute the principal Nb-Ta ore minerals in rare-element pegmatite dykes of the LCT (lithium-cesium-tantalum) petrogenetic family (e.g., [1–9]). The CGM record ore-forming processes, due to their

common occurrence in most pegmatite zones, coupled with complex internal structures and compositional variations in Nb/Ta and Fe/Mn ratios (e.g., [6,10–17]). In general, columbite–tantalite compositions exhibit enrichment in Mn and Ta, with progressive fractionation of granitic-pegmatite-forming melt—fluid systems [1,2,18,19]. In certain Li-rich pegmatites, the composition of columbite–tantalite evolved extensively from columbite-(Fe) to tantalite-(Mn), suggesting the involvement of hydrothermal processes and that the activity of F increased substantially during crystallization [19,20].

The occurrence of CGM, together with other Nb-Ta oxides (e.g., pyrochlore and wodginite group minerals), has attracted significant attention, because they are minerals of economic interest for Ta, hosted in several high-grade deposits worldwide [14,15,18,21]. In general, the Nb-Ta oxide mineral assemblage changes from columbite–tantalite + ixiolite to columbite–tantalite + microlite + ixiolite + cassiterite + wodginite, to microlite + columbite-(Mn), with increasing fractionation.

In this paper, we focus on the internal zoning patterns and major-element compositions of CGM and associated Nb-Ta-Sn oxides in pegmatites from four Li-Be-Ta deposits of the Kolmozero–Voronja zone (Kola region, NW Russia), including two of world-class, with the aim of revealing the ore-forming processes in the Li-rich pegmatite, and deciphering the relationship between pegmatites of different mineralization signatures and ore grade.

2. Geology of the Kola Rare-Metal Pegmatite Belt

The Kola rare-metal pegmatite belt is located in the northeastern part of the Fennoscandian shield in the Kola region, and extends from the Lake Kalmozero to the northwest, almost to the border with Norway. It has a length of more than 300 km and a width of 20 to 45 km. The belt contains up to 95% of granitic pegmatite dikes with rare-metal mineralization (Be, Ta, Nb, Cs, Li) found on the Kola Peninsula [22]. There are six deposits of rare-metal pegmatites within the pegmatite belt. The Polmostundra, Oleniy Ridge, Vasin-Mylk and Okhmylk deposits are confined to the Kolmozero–Voronya greenstone belt. The Kolmozero field is located in the Murmansk province, and the Shongui field is located in the Kola province (Figure 1).

The Murmansk province is dominated by Late Mesoarchean and Neoarchean granites, enderbites, charnockites, and tonalite-trondhjemite gneisses with relics of supracrustal formations. These rocks were metamorphosed under conditions of high-temperature amphibolite facies, and locally contain relics of granulite facies mineral parageneses [23].

The main tectonic units of the Kola Province are the Kola-Norwegian, Keivsky, and Kolmozero–Voronya terranes [24]. The Kola-Norwegian and Keivy terranes are mainly composed of tonalite-trondhjemite-granodiorite gneisses, charnockites and enderbites, metasediments and subordinate amphibolites.

The Kolmozero–Voronya greenstone belt, which was formed 2.92–2.79 Ga ago, is composed of the Polmos-Poros rocks series, represented by four formations (from bottom to top): Lyavozero (lower terrigenous sequence), Polmostundra (komatiite-tholeiite series), Voronietundra (basalt-andesite-dacite series) and Chervutskaya (upper terrigenous sequence). Greenstone rocks were metamorphosed under amphibolite facies conditions [25–27]. The continental crust of the Murmansk and Kola provinces was formed, and underwent significant metamorphic and deformational reworking 2.6–2.9 Ga ago [28].

The main tectonic boundaries of northern Fennoscandia were finally formed in the Paleoproterozoic during the Lapland–Kola collisional orogeny [24,28]. The history of the Lapland–Kola collisional orogen includes intracontinental rifting of the Archean crust (2.5–2.1 Ga), rift opening (~2.1–2.0 Ga), subduction and crustal growth (~2.0–1.9 Ga) intercontinental collision (1.94–1.86 Ga), and orogenic collapse and exhumation (1.90–1.86 Ga). The Kola Province was the northeastern part of the Lapland–Kola Orogen, and underwent Paleoproterozoic deformational reworking, mainly along the boundaries of the main tectonic structures, while the Murmansk Province was practically not affected by Paleoproterozoic deformation [24].

The Kola rare-metal pegmatite belt spatially coincides with the junction zone of the Archean Murmansk and Kola provinces. This junction zone was considered for a long time as an Archean linear mobile-permeable zone (deep fault), which was partially activated in the Paleoproterozoic and is now interpreted as the Kolmozero–Voronya Archean collisional suture [23]. This suture is bordered and penetrated by zones of highly deformed rocks, which are considered to be transcrustal shear zones. Due to their high permeability, these zones were channels through which ore-bearing fluids could circulate. Ore components were deposited both inside the zones and also in the surrounding rocks [29]. The Kolmozero and Polmostundra deposits include albite-spodumene type pegmatites, containing about 20 vol.% [30–32]. The Vasin-Mylk and Okhmylk deposits are complex, and contain the lithium ore minerals spodumene and lepidolite, and the cesium mineral pollucite. The pegmatites of the Shongui deposit are of the beryl type, containing beryl as an accessory ore mineral. For all of the above-mentioned deposits, columbite group minerals occur as accessory minerals, and are of commercial interest, due to the large volumes of the pegmatite ores.

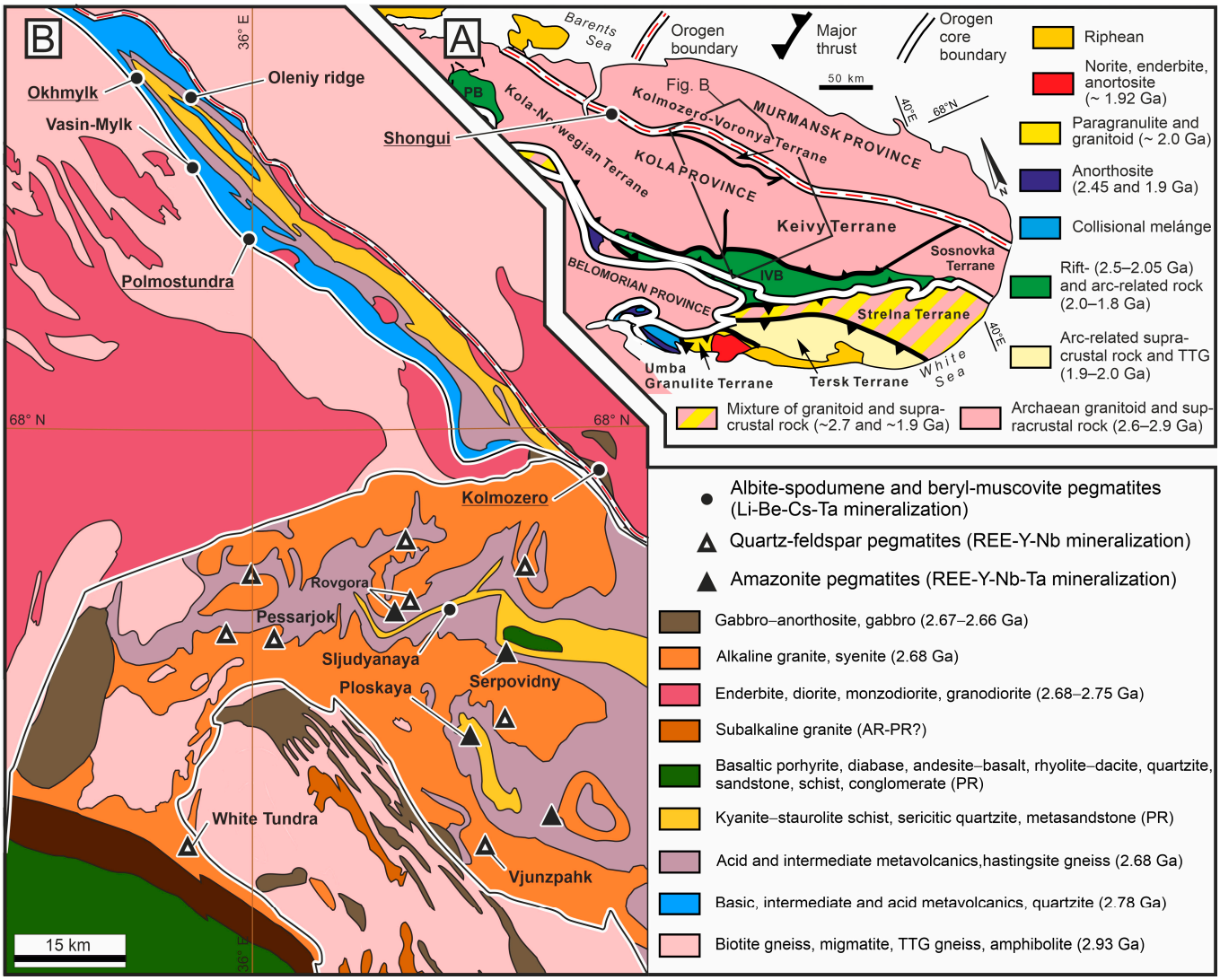


Figure 1. (**A**)—main geological units of the NE Fennoscandian Shield. (**B**)—simplified geological map of the Kola rare-metal pegmatite belt (modified after [22]) with location of deposits (in addition, the Keivy REE-Zr-Nb-Ta pegmatite deposits are shown (see description in [33]). The studied deposits are underlined.

The Kolmozero deposit includes 12 large albite-spodumene pegmatite dykes more than 1400 m long, from 5 to 65 m thick, and are documented to a depth of more than 500 m. The pegmatite dikes are tabular-shaped, and do not show any pronounced concentric zonation. Quartz-plagioclase aplite up to 5 cm thick and coarse-grained quartz-albite aggregates up to 30 cm thick are observed at the contact with the host rocks. The main part of the dikes (85–90%) is composed of coarse-grained quartz-spodumene-feldspar pegmatite. Some domains are composed of a quartz-spodumene aggregate of a coarse-grained structure. The main minerals of the pegmatite are the following (in vol.%): quartz (30–35), albite (30–35), microcline (10–25), spodumene, that is the main lithium mineral (~20), and muscovite (5–7). Accessory minerals include spessartine, apatite, beryl, columbite group minerals, and accessory lithiophilite, triphylite and tourmaline. In total, 64 mineral species have been identified in the pegmatites of the Kolmozero lithium deposit [34]. Columbite-(Mn) from the albite-spodumene pegmatite has yielded a U-Pb age of 2315 ± 10 Ma, which is interpreted as the age of the rare-metal mineralization [35]. This age indicates that the albite-spodumene pegmatites were formed during the Early Paleoproterozoic rifting of the Fennoscandian Shield [36].

The Polmostundra deposit is composed of five tabular-shaped albite-spodumene pegmatite dikes occurring in amphibolites of the Polmostundrovskaya suite of the Kolmozero–Voronya greenstone belt. The pegmatite dikes are 1000–1300 m long, up to 40 m thick, and have been explored to depths of up to 200–300 m. In general, the margins of the pegmatite are composed of granite pegmatite, while aplite occurs along the footwall; however, along the strike and toward depth, both mineralogy and textures show variations. The major minerals of the Polmostundra pegmatites are (in vol.%) quartz (30–50), albite (10–70), spodumene (5–50), and microcline (up to 20). Minor and accessory minerals include muscovite, tourmaline, garnet, apatite, columbite group minerals and beryl. More rare minerals include zeolites, vivianite, sulfides, carbonates, lithiophilite and eucryptite. Holmquistite, biotite, magnetite and epidote group minerals can be observed along the contact with the host amphibolites [22].

The Okhmylk deposit is composed of pegmatite dykes of various thicknesses and lengths, occurring in amphibolites of the Polmostundra Formation of the Kolmozero–Voronya greenstone belt. The length of the dikes varies from 25 to 700 m, and the thickness varies from a few meters to 45 m. The pegmatite dikes show an internal mineralogical and textural zonation. The 0.4 to 4 m-thick marginal part of the dikes (zone 1) at the contact with amphibolite is composed of an aggregate of quartz and feldspar. Minor and accessory minerals include muscovite, black tourmaline, garnet, magnetite and apatite. Towards the center of the dikes, zone 2 is represented by an aggregate of quartz and feldspar, together with columbite group minerals, beryl, garnet, aggregates of apatite and isolated spodumene crystals. Zone 3 is composed of a quartz-albite-spodumene aggregate. The main minerals are (in vol.%) quartz (60–65), spodumene (~20) and albite (10–15). Minor and accessory minerals include tourmaline, beryl, columbite group minerals and microcline. Zone 4 is characterized by blocky quartz and microcline. The major minerals include (in vol.%) microcline (60–70), quartz (15–25) and albite (5–15). Minor and accessory minerals are spodumene (up to 5), polychrome tourmaline, lepidolite, pollucite, muscovite, columbite group minerals, lithiophilite and montebrasite. Recent U-Pb (SHRIMP-RG) geochronological dating of zircon from the Okhmylk pegmatite dyke yielded an age of 2607 ± 9 Ma [37]. We consider this age as the most reliable for the formation of the Li-Cs-Ta pegmatite deposits of the Kolmozero–Voronja belt.

The Shongui deposit consists of three 400 to 1000 m-long and 60 to 80 m-thick pegmatite dikes. The host rocks are amphibolites of the Kola province. The main rock-forming minerals of the dikes are (in vol.%) quartz (30–35), plagioclase (30–35) and microcline (20–25). Accessory minerals include beryl, spodumene, columbite group minerals, tourmaline, muscovite, garnet, zircon, apatite, molybdenite, pyrite, arsenopyrite and ilmenite. About 5 m-thick quartz-albite and quartz-microcline-albite aggregates occur along the margins of the pegmatite dikes, in contact with the host amphibolites. The major volume of the dikes (75–80%) is composed of quartz-microcline and quartz-microcline-albite

aggregates, including domains of quartz-cleavelandite and albite-muscovite-quartz aggregates [38]. The only geochronological determination known from the Shongui pegmatites was performed using the K-Ar method on micas, which gave an age of 2.35–2.10 Ga [39].

Sampled pegmatites from the Kolmozero–Voronja area (i.e., those with economic potential, including the Kolmozero lithium deposit, the Polmostundra lithium-cesium deposit, the Okhmylk lithium deposit and the Shongui beryllium deposit) belong to the LCT petrogenetic family, rare-element class, spodumene and beryl-columbite subtypes (according to the classification of P. Černý and S. Ercit [40]). As no relationships between the studied pegmatites and the pronounced S-type granitic bodies the in region have been established, the anatectic model, rather than the differentiation model, can be applied to explain the formation of these fields. According to the anatectic model, pegmatites are considered to have formed from melts produced by partial melting of suitable lithologies, usually pelitic metasediments and/or metavolcanics (e.g., [41–43]).

3. Sampling and Methods

The studied pegmatite samples (10–12 kg each) were collected from typical rare-element pegmatite dykes (coarse-grained parts) from the Kolmozero–Voronja deposits, which mainly consist of quartz, albite, K-feldspar and spodumene, with minor and accessory muscovite, tourmaline and garnet (Table 1). Based on the Li_2O content, sample KL-GX-11 from Kolmozero is classified as high-grade (>1.5 wt.% Li_2O), sample POL-GX-3/5 from Polmostundra as medium- to-low grade (0.4–1.5 wt.%), while sample OKH-2/2 from Okhmylk is classified as low-grade to barren (<0.4 wt.%). Sample SH-7 from Shongui, which consists mainly of quartz and albite, with minor and accessory beryl, tourmaline, apatite and garnet, shows only traces of Li_2O.

Table 1. Mineralogical and geochemical characterization of the studied samples.

Deposit/Occurrence	Kolmozero	Polmostundra	Okhmylk	Shongui
Sample N	**KL-GX-11**	**POL-GX-3/5**	**OKH-2/2**	**SH-7**
Major and minor minerals (in vol.%)	quartz (50–60); feldspar (microcline + albite) (20–25); spodumene (15–20)	quartz (50–60); feldspar (microcline + albite) (25–30); lepidolite (8–10); spodumene (3–5)	quartz (50–60); feldspar (microcline + albite) (40–45); tourmaline (mainly schorl) (3–5); spodumene (1–2)	quartz (60–65); feldspar (mainly albite) (35–40)
Accessory minerals	garnet, apatite, magnetite, ilmenite	apatite, tourmaline, garnet, magnetite, rutile, ilmenite	apatite, magnetite, garnet	beryl, tourmaline, apatite, garnet, magnetite,
Nb-Ta-Sn oxides	CGM	CGM, pyrochlore/microlite	CGM, pyrochlore, cassiterite	CGM, pyrochlore
Wet chemistry (wt.%)				
SiO2	75.52	75.08	76.10	85.33
TiO2	<0.01	<0.01	0.03	0.02
Al2O3	14.81	12.75	12.10	7.33
Fe2O3	b.d.	0.11	b.d.	0.09
FeO	2.69	1.89	1.57	1.67
MnO	0.11	0.065	0.04	0.18
MgO	0.17	0.08	0.12	0.24
CaO	0.1	0.11	0.23	0.20
Na2O	2.48	3.59	6.11	4.15
K2O	1.25	3.5	2.40	0.17
Li2O	2.27	0.55	0.138	0.005
CO2	0.25	0.02	<0.1	<0.1
F	0.014	0.32	0.017	0.007
Cl	0.005	0.005	0.007	0.011
P2O5	0.08	0.34	0.13	0.10

Table 1. *Cont.*

Deposit/Occurrence	Kolmozero	Polmostundra	Okhmylk	Shongui
Sample N	**KL-GX-11**	**POL-GX-3/5**	**OKH-2/2**	**SH-7**
ICP-MS (ppm)				
Li	11,000	2200	800	29
Be	100	13	7	27
Rb	500	4300	600	11
Nb	49	50	80	23
Sn	30	31	4	1.8
Cs	30	2200	70	17
Ta	17	160	18	8.5
W	1.2	24	1.4	0.3

Note: Wet chemistry analyses (for major elements, using atomic absorption spectrophotometry; TiO_2, using colorimetry; K_2O, Na_2O and Li_2O, using flame photometry; FeO and CO_2, using titration; and F and Cl, using potentiometry, using an ion-selective electrode) were performed in the Geological Institute, Kola Science Centre RAS, Apatity. ICP-MS data were obtained from the Analytical Centre "Geoanalyst" (Zavaritsky Institute of Geology and Geochemistry of the Ural Branch RAS), using the ELAN 9000 quadrupole mass-spectrometer with inductively coupled plasma (PerkinElmer, Shelton, CT, USA) and LSX-500 (Teledyne Technologies, Omaha, NE, USA) attachment for sample laser ablation (for full description, see website on www.geoanalyst.igg.uran.ru (accessed on 1 January 2020)). b.d.—below detection limit.

Although CGM and other Nb-Ta-Sn oxide grains were not directly observed within polished thin sections and hand specimens, the minerals were successfully separated from about 500 g crushed samples, using heavy liquid and a magnetic separator, and by hand-picking under a binocular microscope. Fifteen to twenty-five grains of CGM from each sample were mounted in epoxy resin, and polished using standard methods. As shown in Figures 2–5, the examined CGM grains are anhedral-to-subhedral fragments. The size of the grains varies from 300 to 600 μm.

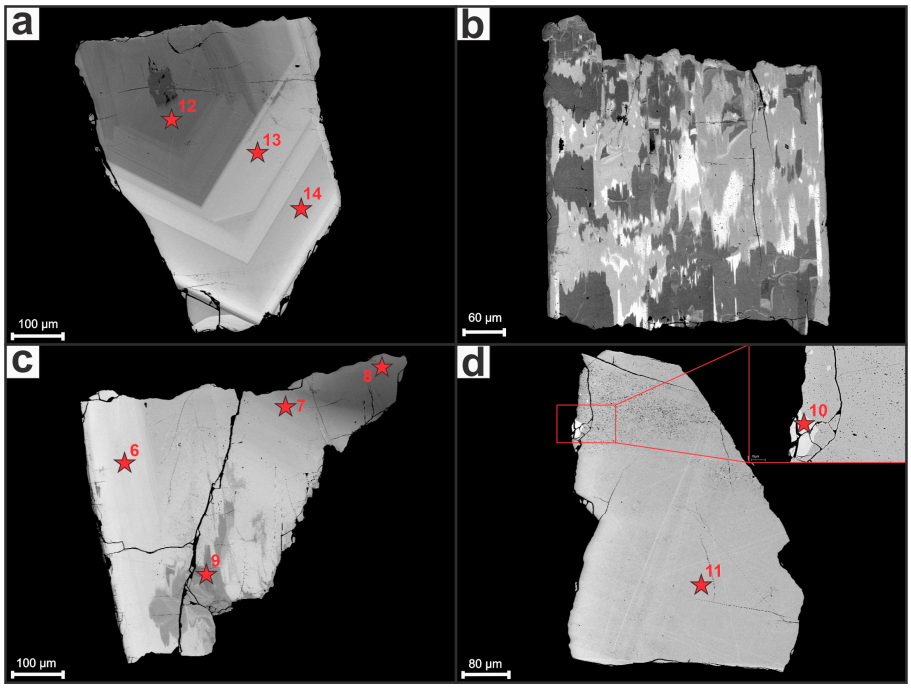


Figure 2. Representative back-scattered electron (BSE) images of CGM grains from the Kolmozero pegmatites, illustrating the internal textures. CGM with normal oscillatory (**a**), patchy (**b**), reverse irregular (**c**), and zoning and homogeneous grain (**d**). Inclusion of rectangular Nb-Ta-Ca-Na-oxide in (**a**) and porous domains (**d**). The numbered red stars indicate points analyzed by microprobe–the numbers (in Figures 2–10) refer to analyses given in Tables 2–4 and Supplementary Materials.

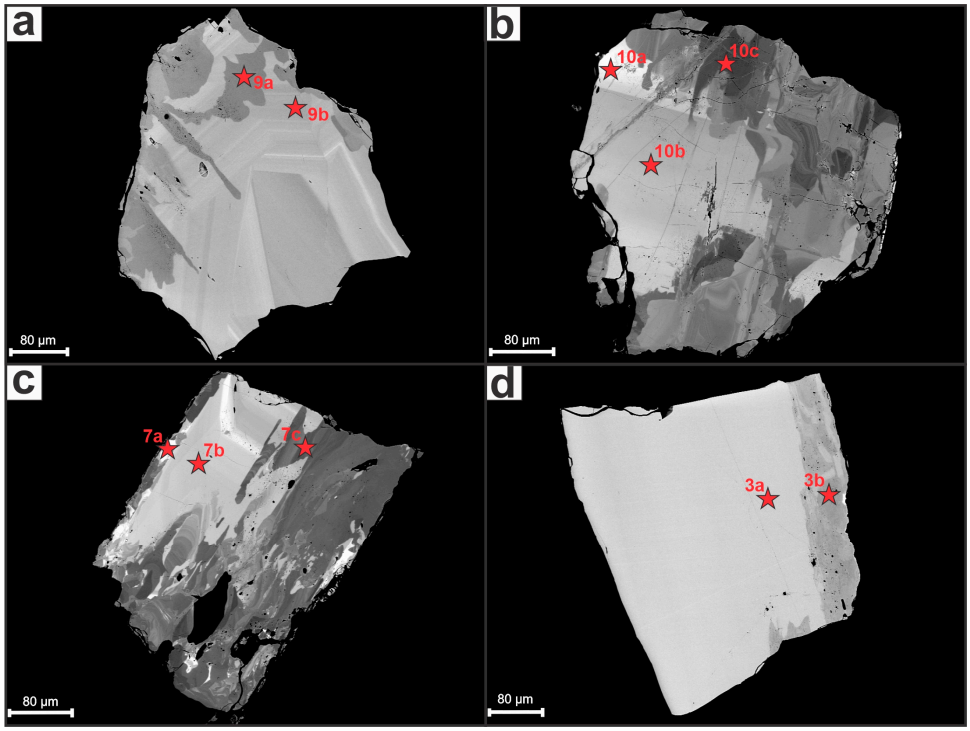


Figure 3. Representative back-scattered electron (BSE) images of CGM grains from the Polmostundra pegmatites, illustrating the internal textures. CGM with mottled (**a**,**b**), patchy (**c**), zoning and homogeneous grain with low BSE intensity, and porous rim (**d**). Internal remnants of CGM with oscillatory zoning (**a**) and homogeneous texture (**b**).

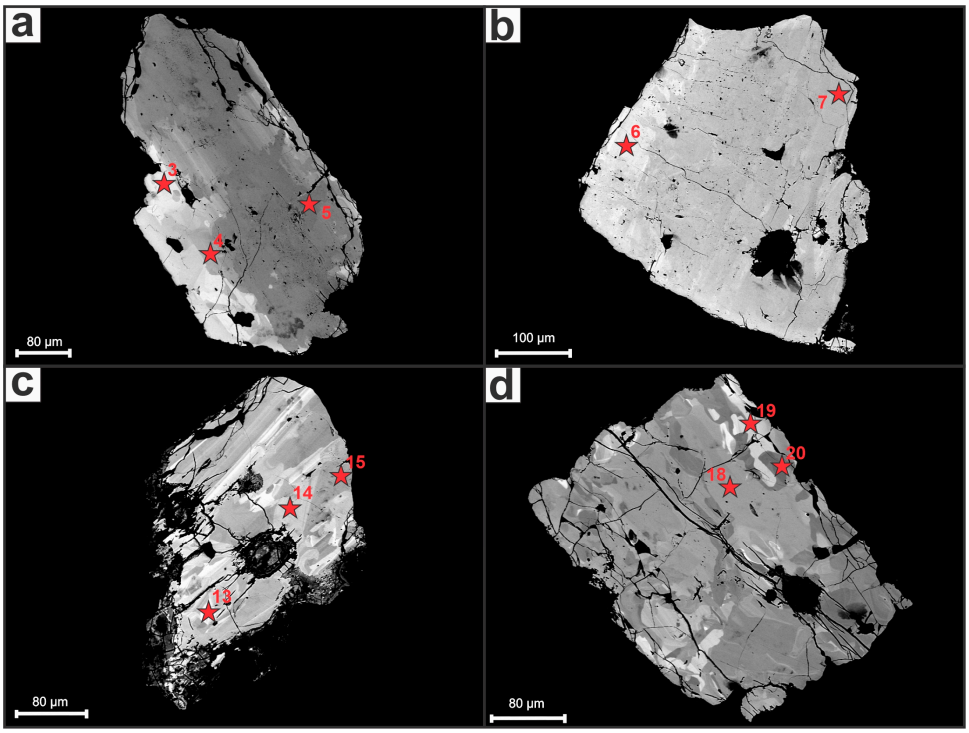


Figure 4. Representative back-scattered electron (BSE) images of CGM grains from the Okhmylk pegmatites, showing variations in the internal textures. CGM with normal irregular (**a**,**b**) and patchy (**c**,**d**) zoning.

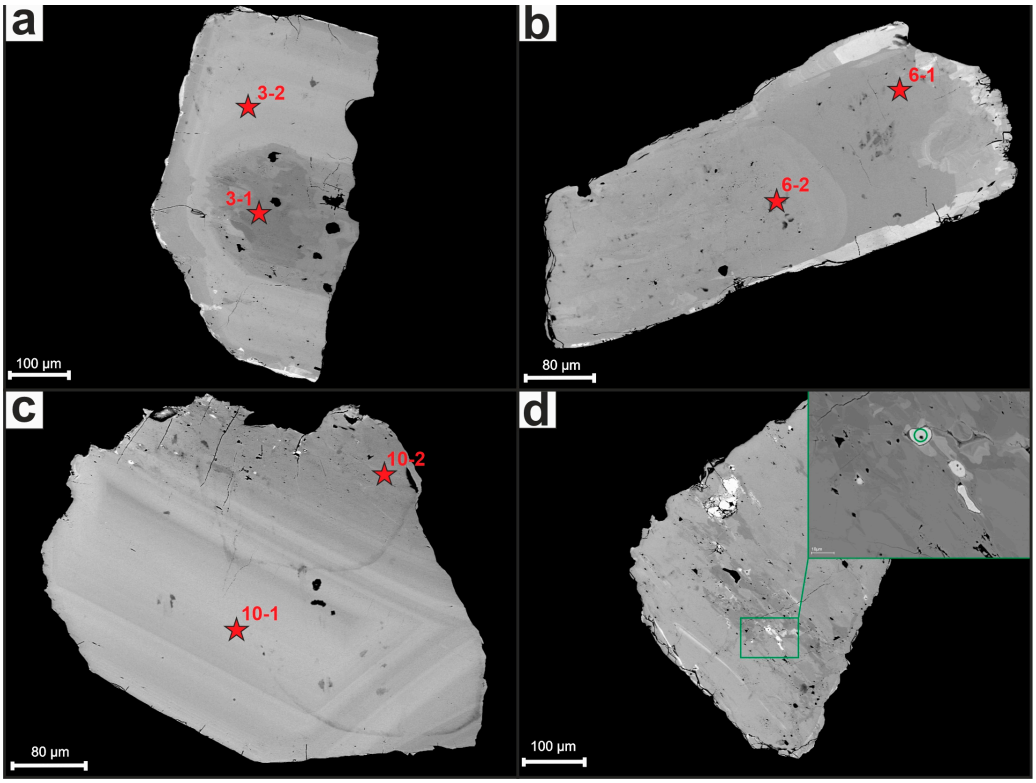


Figure 5. Representative back-scattered electron (BSE) images of CGM grains from the Shongui pegmatites, illustrating the internal textures. CGM with normal irregular zoning (**a**), homogeneous grains with bright thin rims (**b**), transition of oscillatory to homogeneous zoning (**c**), and homogeneous grain with darker core (**d**). Inclusions of Ta-Nb-Ca-Si-Ti-(±Sn) oxide (**d**).

Initially, the sample preparations were studied under a Leo-1450 electron microscope (Carl Zeiss, Göttingen, Germany) with an OXFORD ULTIM MAX 100 energy wavelength dispersive spectrometer (Oxford Instruments, Wisbech, UK) and AZtec software (including elements from C to U). Precise determination of the composition (including elements from Na to U) of all the phases detected under the initial study was carried out using a Cameca MS-46 wave-dispersive electron probe microanalyzer with a probe current of 20–30 nA, an accelerating voltage of 20 kV, and a probe diameter of 5–10 µm. The following natural minerals were used as standards: lorenzenite (Na, Ti), pyrope (Mg, Al), diopside (Si, Ca), fluorapatite (P), barite (S and Ba), atacamite (Cl), wadeite (K), thortveitite (Sc), hematite (Fe), chromite (Cr), celestine (Sr), thorite (Th), lepidolite (Rb), pollucite (Cs), cassiterite (Sn) and uraninite (U). In addition, the following synthetic standards were used: $Y_2Al_5O_{12}$ (Y), $MnCO_3$ (Mn), ZnO (Zn), NiAs (As), $ZrSiO_4$ (Zr), PbTe (Te), $LaCeS_2$ (La, Ce), $LiPr(WO_4)_2$ (Pr), $LiNd(MoO_4)_2$ (Nd), $LiSm(MoO_4)_2$ (Sm), $LiEu(MoO_4)_2$ (Eu), $LiGd(MoO_4)_2$ (Gd), $LiDy(WO_4)_2$ (Dy), PbSe (Pb), and metallic vanadium, cobalt, nickel, copper, hafnium, niobium, tantalum, molybdenum, palladium, platinum, gold, silver, bismuth, antimony and tungsten.

A total of 102 compositions of Nb-Ta-Sn oxides were obtained using an electron probe microanalyzer. Representative chemical analyzes of CGM, pyrochlore super-group minerals (PSGM) and cassiterite are given in Tables 2–4; the whole data set (including relevant BSE images) is given in the Supplementary Materials.

Table 2. Representative compositions of CGM from the Kolmozero, Polmostundra, Okhmylk and Shongui pegmatites.

	Kolmozero										
Sample #	**6**	**7**	**8**	**9**	**10**	**11**	**12**	**13**	**14**	**19**	**20**
MgO	0.07	0.06	0.05	0.00	0.06	b.d.	b.d.	b.d.	0.07	b.d.	b.d.
Al_2O_3	b.d.	b.d.	b.d.	b.d.	b.d.	0.07	b.d.	b.d.	b.d.	b.d.	b.d.
SiO_2	0.79	0.61	0.36	0.52	1.40	0.92	0.25	0.47	0.39	0.17	0.22
CaO	0.06	0.05	0.05	0.05	0.14	0.05	0.19	0.09	0.04	b.d.	b.d.
TiO_2	0.75	0.60	0.46	0.48	0.90	0.78	0.49	0.46	0.47	0.29	0.44
V_2O_5	b.d.	b.d.	b.d.	b.d.	b.d.	b.d.	b.d.	b.d.	b.d.	0.07	0.08
MnO	7.44	7.79	8.66	8.45	2.78	8.18	8.54	11.20	7.98	11.11	11.08
FeO	8.94	9.45	10.37	9.57	12.30	7.87	10.28	9.46	10.00	8.43	8.54
ZnO	0.17	0.12	0.07	0.13	0.13	0.20	b.d.	0.11	0.13	b.d.	b.d.
ZrO_2	b.d.	b.d.	b.d.	b.d.	b.d.	b.d.	b.d.	b.d.	b.d.	b.d.	b.d.
Nb_2O_5	16.68	26.22	42.85	34.02	11.85	13.89	56.78	40.56	41.87	54.20	52.83
SnO_2	b.d.	b.d.	b.d.	b.d.	0.50	0.33	b.d.	b.d.	b.d.	b.d.	b.d.
Ta_2O_5	64.08	53.97	35.40	46.12	69.99	67.62	21.92	37.37	38.28	24.03	24.57
WO_3	0.40	0.25	0.24	0.24	0.44	0.36	b.d.	0.27	0.43	b.d.	0.61
UO_2	b.d.	b.d.	b.d.	b.d.	b.d.	b.d.	b.d.	b.d.	b.d.	b.d.	b.d.
Sc_2O_3											
Total	99.38	99.12	98.50	99.58	100.49	100.26	98.45	99.99	99.66	98.30	98.35
Zoning	p	p	p	p	r	h (porous)	o	o	o	h	h
	Formulae on basis of 6 oxygens										
Si	0.059	0.044	0.024	0.036	0.106	0.070	0.015	0.031	0.026	0.011	0.014
Al	0.000	0.000	0.000	0.000	0.000	0.006	0.000	0.000	0.000	0.000	0.000
Ti	0.043	0.032	0.023	0.025	0.051	0.044	0.023	0.023	0.023	0.014	0.021
Fe^{2+}	0.564	0.569	0.576	0.552	0.783	0.499	0.536	0.524	0.554	0.445	0.453
Mn	0.476	0.475	0.488	0.493	0.179	0.526	0.451	0.628	0.448	0.595	0.595
Mg	0.008	0.006	0.005	0.000	0.007	0.000	0.000	0.000	0.007	0.000	0.000
Zn	0.010	0.006	0.004	0.007	0.007	0.011	0.000	0.005	0.006	0.000	0.000
Ca	0.005	0.004	0.003	0.003	0.011	0.004	0.012	0.007	0.003	0.000	0.000
Nb	0.569	0.853	1.288	1.060	0.408	0.477	1.599	1.214	1.254	1.548	1.514
Ta	1.315	1.056	0.640	0.864	1.449	1.396	0.371	0.673	0.690	0.413	0.424
U	0.000	0.000	0.000	0.000	0.000	0.000	0.000	0.000	0.000	0.000	0.000
Sn	0.000	0.000	0.000	0.000	0.015	0.010	0.000	0.000	0.000	0.000	0.000
W	0.008	0.005	0.004	0.004	0.009	0.007	0.000	0.005	0.007	0.000	0.010
V	0.000	0.000	0.000	0.000	0.000	0.000	0.000	0.000	0.000	0.002	0.002
Sc											
Site A (Fe + Mn + Mg + Zn + Ca)	1.062	1.060	1.075	1.055	1.002	1.051	0.999	1.163	1.018	1.040	1.048
Site B (Nb + Ta + Si + W + Sn + V + Ti)	1.986	1.986	1.974	1.985	2.014	1.986	2.008	1.940	1.994	1.987	1.974
Ta/(Ta + Nb)	0.698	0.553	0.332	0.449	0.780	0.745	0.188	0.357	0.355	0.211	0.219
Mn/(Mn + Fe)	0.457	0.455	0.458	0.472	0.186	0.513	0.457	0.545	0.447	0.572	0.568

Table 2. *Cont.*

Sample #	**Polmostundra**									
	3a	**3b**	**7a**	**7b**	**7c**	**9a**	**9b**	**10a**	**10b**	**10c**
MgO	0.11	b.d.	0.08	b.d.	0.10	0.15	0.11	0.09	0.13	b.d.
Al_2O_3	b.d.	b.d.	b.d.	b.d.	b.d.	b.d.	b.d.	b.d.	b.d.	b.d.
SiO_2	0.18	0.10	0.69	0.51	0.17	0.10	0.17	0.65	0.39	0.08
CaO	b.d.	b.d.	b.d.	b.d.	b.d.	b.d.	b.d.	b.d.	b.d.	b.d.
TiO_2	0.41	1.01	0.77	0.41	0.76	0.78	0.57	1.07	0.63	0.88
V_2O_5	b.d.	b.d.	b.d.	b.d.	b.d.	b.d.	b.d.	0.06	b.d.	b.d.
MnO	4.49	6.87	4.80	5.39	3.61	4.54	5.95	6.18	4.23	4.55
FeO	15.70	13.89	12.33	12.02	16.53	16.06	14.43	13.08	14.34	15.80
ZnO	b.d.	b.d.	0.16	0.11	0.11	b.d.	b.d.	0.13	0.10	b.d.
ZrO_2	b.d.	b.d.	b.d.	b.d.	b.d.	b.d.	b.d.	b.d.	b.d.	b.d.
Nb_2O_5	61.84	67.68	38.57	42.83	60.60	68.52	62.35	36.04	47.08	68.73
SnO_2	b.d.	b.d.	0.45	0.31	b.d.	b.d.	b.d.	0.84	0.35	b.d.
Ta_2O_5	14.90	8.90	39.75	36.11	16.76	8.22	14.55	39.17	30.12	8.13
WO_3	0.30	0.45	0.41	0.53	0.38	0.41	0.53	0.54	0.54	0.34
UO_2	b.d.	b.d.	b.d.	b.d.	b.d.	b.d.	b.d.	b.d.	b.d.	b.d.
Sc_2O_3										
Total	97.92	98.89	98.01	98.23	99.03	98.77	98.66	97.86	97.90	98.52
Zoning	h	h (reverse)	p	p	p	m	o	r	h	m
Formulae on basis of 6 oxygens										
Si	0.011	0.006	0.047	0.034	0.011	0.006	0.010	0.044	0.025	0.005
Al	0.000	0.000	0.000	0.000	0.000	0.000	0.000	0.000	0.000	0.000
Ti	0.019	0.044	0.039	0.021	0.035	0.034	0.026	0.055	0.031	0.039
Fe^{2+}	0.801	0.683	0.700	0.670	0.840	0.788	0.730	0.747	0.783	0.777
Mn	0.232	0.342	0.276	0.305	0.186	0.226	0.305	0.357	0.234	0.227
Mg	0.010	0.000	0.008	0.000	0.009	0.013	0.010	0.009	0.012	0.000
Zn	0.000	0.000	0.008	0.005	0.005	0.000	0.000	0.007	0.005	0.000
Ca	0.000	0.000	0.000	0.000	0.000	0.000	0.000	0.000	0.000	0.000
Nb	1.706	1.799	1.183	1.291	1.664	1.818	1.704	1.113	1.389	1.827
Ta	0.247	0.142	0.733	0.655	0.277	0.131	0.239	0.727	0.535	0.130
U	0.000	0.000	0.000	0.000	0.000	0.000	0.000	0.000	0.000	0.000
Sn	0.000	0.000	0.012	0.008	0.000	0.000	0.000	0.023	0.009	0.000
W	0.005	0.007	0.007	0.009	0.006	0.006	0.008	0.010	0.009	0.005
V	0.000	0.000	0.000	0.000	0.000	0.000	0.000	0.001	0.000	0.000
Sc	0.000	0.000	0.000	0.000	0.000	0.000	0.000	0.000	0.000	0.000
Site A (Fe + Mn + Mg + Zn + Ca)	1.043	1.025	0.992	0.980	1.040	1.027	1.044	1.120	1.034	1.004
Site B (Nb + Ta + Si + W + Sn + V + Ti)	1.983	1.992	2.014	2.009	1.986	1.990	1.980	1.963	1.989	2.001
Ta/(Ta + Nb)	0.127	0.073	0.383	0.337	0.143	0.067	0.123	0.395	0.278	0.066
Mn/(Mn + Fe)	0.225	0.334	0.283	0.312	0.181	0.223	0.294	0.324	0.230	0.226

Table 2. *Cont.*

Sample #	Okhmylk									
	3	**4**	**5**	**6**	**7**	**13**	**14**	**15**	**18**	**19**
MgO	b.d.	b.d.	b.d.	b.d.	b.d.	b.d.	b.d.	b.d.	b.d.	b.d.
Al_2O_3	0.04	b.d.	b.d.	b.d.	0.07	b.d.	b.d.	b.d.	b.d.	b.d.
SiO_2	0.26	0.16	0.10	0.13	0.14	0.23	b.d.	0.17	0.17	0.33
CaO	b.d.	0.06	b.d.	b.d.	b.d.	b.d.	b.d.	b.d.	b.d.	b.d.
TiO_2	0.09	0.35	0.56	0.52	0.58	0.10	0.22	0.09	0.12	0.15
V_2O_5	b.d.	b.d.	b.d.	b.d.	b.d.	b.d.	b.d.	b.d.	b.d.	b.d.
MnO	15.47	16.14	12.98	7.85	10.77	16.06	17.65	17.52	15.59	14.56
FeO	3.92	3.47	8.00	12.83	8.30	3.17	1.85	1.53	3.96	4.26
ZnO	b.d.	0.02	b.d.	b.d.	b.d.	b.d.	b.d.	b.d.	b.d.	b.d.
ZrO_2	b.d.	b.d.	b.d.	b.d.	b.d.	b.d.	b.d.	b.d.	b.d.	b.d.
Nb_2O_5	54.44	62.17	66.94	61.59	67.03	53.70	56.61	64.37	54.26	51.93
SnO_2	b.d.	b.d.	b.d.	b.d.	b.d.	b.d.	b.d.	b.d.	b.d.	b.d.
Ta_2O_5	23.31	16.13	10.77	14.41	12.53	25.05	20.87	16.77	22.70	26.91
WO_3	0.47	0.84	0.73	1.15	0.86	0.36	0.50	0.38	0.42	0.43
UO_2	0.15	b.d.	b.d.	b.d.	b.d.	n.a.	n.a.	n.a.	n.a.	n.a.
Sc_2O_3	b.d.	0.15	0.16	0.18	0.23	0.11	0.14	0.08	0.10	0.14
Total	98.14	99.49	100.24	98.66	100.51	98.77	97.84	100.92	97.32	98.71
Zoning	p (rim)	p (interm)	p (core)	r	ce	p	p	p	p (core)	p (rim)
	Formulae on basis of 6 oxygens									
Si	0.016	0.010	0.006	0.008	0.008	0.014	0.000	0.010	0.011	0.021
Al	0.003	0.000	0.000	0.000	0.005	0.000	0.000	0.000	0.000	0.000
Ti	0.004	0.016	0.025	0.024	0.026	0.005	0.010	0.004	0.005	0.007
Fe^{2+}	0.205	0.175	0.389	0.644	0.411	0.167	0.097	0.077	0.209	0.226
Mn	0.821	0.824	0.639	0.399	0.540	0.855	0.933	0.888	0.833	0.783
Mg	0.000	0.000	0.000	0.000	0.000	0.000	0.000	0.000	0.000	0.000
Zn	0.000	0.000	0.000	0.000	0.000	0.000	0.000	0.000	0.000	0.000
Ca	0.000	0.004	0.000	0.000	0.000	0.000	0.000	0.000	0.000	0.000
Nb	1.543	1.694	1.760	1.672	1.795	1.526	1.597	1.742	1.547	1.491
Ta	0.397	0.264	0.170	0.235	0.202	0.428	0.354	0.273	0.389	0.465
U	0.002	0.000	0.000	0.000	0.000	0.000	0.000	0.000	0.000	0.000
Sn	0.000	0.000	0.000	0.000	0.000	0.000	0.000	0.000	0.000	0.000
W	0.008	0.013	0.011	0.018	0.013	0.006	0.008	0.006	0.007	0.007
V	0.000	0.000	0.000	0.000	0.000	0.000	0.000	0.000	0.000	0.000
Sc	0.000	0.004	0.004	0.005	0.006	0.003	0.004	0.002	0.003	0.004
Site A (Fe + Mn + Mg + Zn + Ca)	1.027	1.003	1.028	1.043	0.952	1.022	1.030	0.965	1.041	1.009
Site B (Nb + Ta + Si + W + Sn + V + Ti)	1.961	1.984	1.961	1.939	2.031	1.973	1.962	2.029	1.952	1.984
Ta/(Ta + Nb)	0.205	0.135	0.088	0.123	0.101	0.219	0.182	0.135	0.201	0.238
Mn/(Mn + Fe)	0.800	0.825	0.622	0.383	0.568	0.837	0.906	0.921	0.800	0.776

Table 2. *Cont.*

Sample #	Shongui							
	3-1	**3-2**	**6-1**	**6-2**	**7-1**	**7-2**	**10-1**	**10-2**
MgO	0.07	b.d.	b.d.	b.d.	b.d.	b.d.	0.10	b.d.
Al_2O_3	b.d.	b.d.	b.d.	b.d.	1.72	b.d.	b.d.	b.d.
SiO_2	b.d.	b.d.	0.10	0.09	0.30	0.13	0.22	0.12
CaO	b.d.	b.d.	b.d.	b.d.	b.d.	b.d.	b.d.	b.d.
TiO_2	2.12	1.05	0.50	0.60	0.61	0.60	1.50	1.69
V_2O_5	b.d.	b.d.	b.d.	b.d.	b.d.	b.d.	b.d.	b.d.
MnO	6.13	6.67	8.06	7.91	10.20	7.29	6.39	8.82
FeO	13.83	12.98	12.34	12.84	9.29	12.87	13.27	11.21
ZnO	0.04	b.d.	b.d.	b.d.	b.d.	b.d.	b.d.	b.d.
ZrO_2	b.d.	b.d.	b.d.	b.d.	b.d.	b.d.	b.d.	b.d.
Nb_2O_5	67.42	62.36	62.45	60.75	51.71	60.63	54.88	58.08
SnO_2	0.20	b.d.	b.d.	b.d.	b.d.	b.d.	b.d.	b.d.
Ta_2O_5	8.04	15.53	15.04	16.21	24.96	16.84	22.49	17.64
WO_3	0.30	b.d.	b.d.	b.d.	b.d.	b.d.	b.d.	b.d.
UO_2	b.d.	b.d.	b.d.	b.d.	b.d.	b.d.	b.d.	b.d.
Sc_2O_3	0.40	0.20	b.d.	b.d.	b.d.	b.d.	0.25	0.36
Total	98.55	98.79	98.48	98.39	98.80	98.35	99.08	97.93
Zoning	c	r	h	h	r	h	o	o
	Formulae on basis of 6 oxygens							
Si	0.000	0.000	0.006	0.005	0.018	0.008	0.013	0.007
Al	0.000	0.000	0.000	0.000	0.123	0.000	0.000	0.000
Ti	0.093	0.048	0.023	0.027	0.028	0.027	0.069	0.077
Fe^{2+}	0.676	0.655	0.620	0.646	0.472	0.652	0.680	0.571
Mn	0.303	0.341	0.410	0.403	0.525	0.374	0.332	0.455
Mg	0.006	0.000	0.000	0.000	0.000	0.000	0.009	0.000
Zn	0.002	0.000	0.000	0.000	0.000	0.000	0.000	0.000
Ca	0.000	0.000	0.000	0.000	0.000	0.000	0.000	0.000
Nb	1.782	1.701	1.696	1.653	1.421	1.661	1.522	1.598
Ta	0.128	0.255	0.246	0.265	0.413	0.278	0.375	0.292
U	0.000	0.000	0.000	0.000	0.000	0.000	0.000	0.000
Sn	0.005	0.000	0.000	0.000	0.000	0.000	0.000	0.000
W	0.005	0.000	0.000	0.000	0.000	0.000	0.000	0.000
V	0.000	0.000	0.000	0.000	0.000	0.000	0.000	0.000
Sc	0.010	0.005	0.000	0.000	0.000	0.000	0.007	0.010
Site A (Fe + Mn + Mg + Zn + Ca)	0.988	0.996	1.030	1.049	0.997	1.026	1.021	1.025
Site B (Nb + Ta + Si + W + Sn + V + Ti)	2.008	2.004	1.970	1.951	1.879	1.974	1.979	1.975
Ta/(Ta + Nb)	0.067	0.130	0.127	0.138	0.225	0.143	0.198	0.154
Mn/(Mn + Fe)	0.310	0.342	0.398	0.384	0.526	0.364	0.328	0.443

Note. b.d.—below detection limit; n.a.—not analyzed; p—patchy; r—overgrowing rim; o—oscillatory; h—homogeneous; m—mottled; c—core.

Table 3. Representative compositions of PSGM from the Polmostundra, Okhmylk and Shongui pegmatites.

Sample #	Polmostundra									
	Pcl 1	**Pcl 2**	**Pcl 3**	**Pcl 4**	**Pcl 5**	**Pcl 6**	**Pcl 7**	**Pcl 8**	**3-4**	**3-5**
Na_2O	4.77	5.18	5.26	5.43	4.71	5.22	4.57	5.20	3.04	2.57
MgO	b.d.	b.d.	b.d.	b.d.	0.06	b.d.	b.d.	b.d.	n.a.	n.a.
Al_2O_3	b.d.	b.d.	0.04	0.03	b.d.	b.d.	b.d.	b.d.	b.d.	b.d.
SiO_2	n.a.	n.a.	n.a.	n.a.	n.a.	n.a.	n.a.	n.a.	n.a.	n.a.
K_2O	b.d.	b.d.	b.d.	b.d.	b.d.	b.d.	b.d.	b.d.		0.25
CaO	7.73	6.17	7.78	7.52	6.98	8.28	8.63	7.09	4.47	1.95
TiO_2	b.d.	b.d.	b.d.	b.d.	b.d.	b.d.	b.d.	b.d.	n.a.	n.a.
MnO	b.d.	b.d.	0.11	b.d.	0.22	b.d.	0.14	0.17	n.a.	0.18
FeO	b.d.	b.d.	b.d.	b.d.	b.d.	b.d.	b.d.	b.d.	n.a.	n.a.
As_2O_3	n.a.	n.a.	n.a.	n.a.	n.a.	n.a.	n.a.	n.a.	n.a.	n.a.
SrO	2.78	1.76	1.09	1.36	0.88	1.15	1.29	2.01	n.a.	n.a.
Y_2O_3	n.a.	n.a.	n.a.	n.a.	n.a.	n.a.	n.a.	n.a.	3.04	n.a.
Nb_2O_5	1.97	2.18	1.26	2.52	2.27	2.00	2.63	2.36	2.11	2.22
SnO_2	b.d.	0.28	0.30	0.81	1.13	0.34	0.66	0.55	n.a.	n.a.
Ta_2O_5	78.53	75.79	76.72	72.12	70.30	78.07	72.37	73.19	71.80	76.68
WO_3	0.70	1.20	0.68	1.03	0.96	0.96	1.11	1.02	8.80	6.51
PbO	b.d.	1.07	1.54	1.60	2.81	0.58	1.45	2.04	2.83	3.95
ThO_2	0.60	b.d.	b.d.	b.d.	b.d.	b.d.	0.31	b.d.	0.01	b.d.
UO_2	b.d.	2.55	2.25	5.80	7.24	1.02	3.51	4.58	4.84	3.37
F	2.36	1.59	1.94	1.73	1.22	2.28	1.93	2.09	b.d.	
Total	99.44	97.76	98.95	99.93	98.76	99.90	98.59	100.29	100.94	97.68
O=F	0.99	0.67	0.82	0.73	0.51	0.96	0.81	0.88	n.a.	n.a.
H_2Ocalc	0.56	0.90	0.71	0.78	0.98	0.61	0.69	0.62	1.71	1.77
Total	99.00	97.99	98.85	99.99	99.23	99.54	98.47	100.03	102.65	99.45
	Formulae on basis of B = 2 cations									
Na	0.825	0.913	0.937	0.986	0.876	0.899	0.828	0.940	0.518	0.423
K	0.000	0.000	0.000	0.000	0.000	0.000	0.000	0.000		0.014
Ca	0.738	0.600	0.766	0.754	0.718	0.788	0.863	0.708	0.421	0.177
Mn	0.000	0.000	0.008	0.000	0.018	0.000	0.011	0.013		0.013
Fe										
Sr	0.144	0.093	0.058	0.074	0.049	0.059	0.070	0.108		
As										
Y									0.31	
Pb	0.000	0.026	0.038	0.040	0.073	0.014	0.036	0.051	0.067	0.090
Th	0.012	0.000	0.000	0.000	0.000	0.000	0.007	0.000		
U	0.000	0.051	0.046	0.121	0.155	0.020	0.073	0.095	0.095	0.064
∑A	1.719	1.683	1.854	1.975	1.896	1.781	1.888	1.916	1.101	0.781
Mg	0.000	0.000	0.000	0.000	0.008	0.000	0.000	0.000		
Al	0.000	0.000	0.004	0.003	0.000	0.000	0.000	0.000		

Table 3. *Cont.*

Sample #	Polmostundra									
	Pcl 1	**Pcl 2**	**Pcl 3**	**Pcl 4**	**Pcl 5**	**Pcl 6**	**Pcl 7**	**Pcl 8**	**3-4**	**3-5**
Si										
Ti	0.000	0.000	0.000	0.000	0.000	0.000	0.000	0.000		
Nb	0.079	0.089	0.052	0.107	0.098	0.080	0.111	0.099	0.084	0.085
Sn	0.000	0.010	0.011	0.030	0.043	0.012	0.025	0.021		
Ta	1.904	1.872	1.917	1.835	1.835	1.886	1.838	1.855	1.716	1.771
W	0.016	0.028	0.016	0.025	0.024	0.022	0.027	0.025	0.2	0.143
∑B	2.000	2.000	2.000	2.000	2.000	2.000	2.000	2.000	2.000	1.999
F	0.666	0.457	0.564	0.512	0.370	0.641	0.570	0.616	0.000	0.000
OH	0.334	0.543	0.436	0.488	0.630	0.359	0.430	0.384	1.000	1.000
Vacancy	0.281	0.317	0.146	0.025	0.104	0.219	0.112	0.084	0.899	1.219
Sample #	**Okhmylk**								**Shongui**	
	10	**12**	**10a**	**13**	**14**	**12a**	**15**	**16**	**1**	**2**
Na_2O	n.a.	n.a.	n.a.	n.a.	n.a.	n.a.	n.a.	n.a.	0.62	1.55
MgO	b.d.	b.d.	b.d.	b.d.	b.d.	b.d.	b.d.	b.d.	0.08	0.10
Al_2O_3	b.d.	b.d.	b.d.	b.d.	0.03	b.d.	b.d.	b.d.	0.17	0.03
SiO_2	0.09	b.d.	0.13	0.16	b.d.	b.d.	b.d.	b.d.	5.81	6.41
K_2O	n.a.	n.a.	n.a.	n.a.	n.a.	n.a.	n.a.	n.a.	n.a.	n.a.
CaO	15.76	15.43	14.88	15.99	15.74	15.38	15.63	15.12	16.18	15.76
TiO_2	0.20	0.20	0.24	0.22	0.20	0.26	0.15	0.23	4.25	2.64
MnO	0.35	6.28	0.67	0.37	0.31	0.78	0.58	0.65	0.60	0.44
FeO	b.d.	b.d.	0.15	b.d.	b.d.	0.22	0.28	0.25	1.33	0.68
As_2O_3	n.a.	n.a.	n.a.	n.a.	n.a.	n.a.	n.a.	n.a.	3.75	1.98
SrO	n.a.	n.a.	n.a.	n.a.	n.a.	n.a.	n.a.	n.a.	n.a.	n.a.
Y_2O_3	n.a.	n.a.	0.40	0.44	0.44	0.28	0.37	0.32	n.a.	n.a.
Nb_2O_5	66.90	61.54	64.58	67.09	65.74	62.21	64.52	63.18	16.27	12.02
SnO_2	b.d.	b.d.	n.a.	n.a.	n.a.	n.a.	n.a.	n.a.	0.93	1.73
Ta_2O_5	13.42	13.75	14.36	13.89	14.69	14.62	13.86	14.12	40.54	50.67
WO_3	b.d.	b.d.	b.d.	b.d.	b.d.	b.d.	b.d.	b.d.	n.a.	n.a.
PbO	n.a.	n.a.	n.a.	n.a.	n.a.	n.a.	n.a.	n.a.	n.a.	n.a.
ThO_2	n.a.	n.a.	n.a.	n.a.	n.a.	n.a.	n.a.	n.a.	n.a.	n.a.
UO_2	n.a.	n.a.	b.d.	b.d.	b.d.	b.d.	b.d.	b.d.	0.43	0.59
F	b.d.	b.d.	b.d.	b.d.	b.d.	b.d.	b.d.	b.d.	b.d.	b.d.
Total	96.72	97.20	95.41	98.16	97.13	93.75	95.39	93.88	90.96	94.60
O=F										
H_2Ocalc	2.56	2.34	2.50	2.58	2.54	2.42	2.48	2.44	2.62	2.31
Total	99.28	99.53	97.91	100.74	99.67	96.17	97.87	96.32	93.58	96.91
	Formulae on basis of B = 2 cations									
Na									0.08	0.20
K										
Ca	0.989	1.043	0.955	0.995	0.995	1.021	1.014	0.995	1.149	1.096

Table 3. *Cont.*

Sample #	Okhmylk								Shongui	
	10	**12**	**10a**	**13**	**14**	**12a**	**15**	**16**	**1**	**2**
Mn	0.018	0.335	0.034	0.018	0.015	0.041	0.030	0.034	0.034	0.024
Fe	0.000	0.000	0.007	0.000	0.000	0.011	0.014	0.013	0.074	0.037
Sr										
As									0.151	0.078
Y			0.013	0.014	0.014	0.009	0.012	0.010		
Pb									0.000	0.000
Th										
U		0.000	0.000	0.000	0.000	0.000	0.000	0.000	0.006	0.009
∑A	1.007	1.378	1.009	1.027	1.024	1.082	1.070	1.052	1.494	1.439
Mg	0.000	0.000	0.000	0.000	0.000	0.000	0.000	0.000	0.008	0.010
Al	0.000	0.000	0.000	0.000	0.002	0.000	0.000	0.000	0.013	0.002
Si	0.005	0.000	0.008	0.009	0.000	0.000	0.000	0.000	0.525	0.567
Ti	0.009	0.009	0.011	0.010	0.009	0.012	0.007	0.011	0.212	0.129
Nb	1.772	1.755	1.748	1.762	1.754	1.742	1.765	1.754	0.487	0.353
Sn	0.000	0.000							0.025	0.045
Ta	0.214	0.236	0.234	0.219	0.236	0.246	0.228	0.236	0.730	0.894
W	0.000	0.000	0.000	0.000	0.000	0.000	0.000	0.000		
∑B	2.000	2.000	2.001	2.000	2.001	2.000	2.000	2.001	2.000	2.000
F	0.000	0.000	0.000	0.000	0.000	0.000	0.000	0.000	0.000	0.000
OH	1.000	1.000	1.000	1.000	1.000	1.000	1.000	1.000	1.000	1.000
Vacancy	0.993	0.622	0.991	0.973	0.976	0.918	0.930	0.948	0.506	0.561

Note. b.d.—below detection limit, n.a.—not analyzed.

Table 4. Representative compositions of cassiterite from the Okhmylk pegmatite.

Sample #	**2**	**3**	**4**	**5**	**6**	**7**	**8**	**9**	**10**
MgO	b.d.	b.d.	b.d.	b.d.	b.d.	b.d.	b.d.	b.d.	b.d.
Al_2O_3	0.09	0.07	0.13	0.09	b.d.	b.d.	b.d.	b.d.	0.09
SiO_2	0.27	0.26	0.28	0.27	0.18	0.29	0.26	0.31	0.29
TiO_2	b.d.	b.d.	b.d.	b.d.	b.d.	b.d.	b.d.	b.d.	b.d.
MnO	b.d.	b.d.	b.d.	b.d.	b.d.	b.d.	b.d.	b.d.	b.d.
FeO	0.20	0.59	0.26	0.15	b.d.	b.d.	b.d.	0.22	b.d.
ZrO_2	b.d.	b.d.	b.d.	b.d.	b.d.	b.d.	b.d.	b.d.	b.d.
Nb_2O_5	b.d.	0.65	b.d.	0.40	0.37	b.d.	0.12	0.26	b.d.
SnO_2	98.68	94.21	97.78	98.52	98.89	99.61	99.62	98.03	98.46
Ta_2O_5	0.52	3.93	1.53	0.68	0.73	b.d.	0.55	0.83	0.50
WO_3	b.d.	b.d.	b.d.	b.d.	b.d.	b.d.	b.d.	b.d.	b.d.
Total	99.76	99.71	99.97	100.11	100.17	99.89	100.54	99.65	99.33

Note. b.d.—below detection limit.

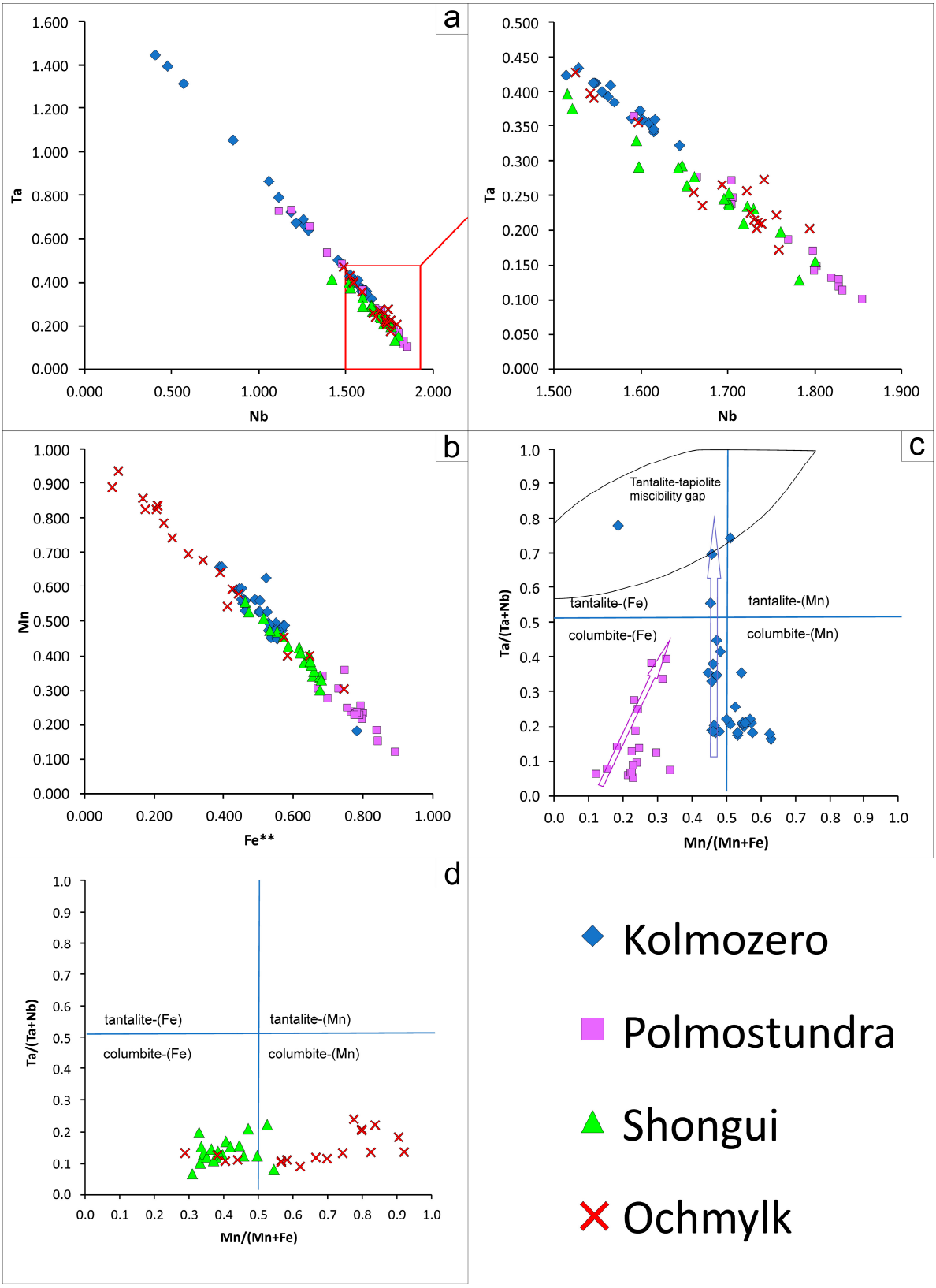


Figure 6. Major-element compositions in CGM from the Kolmozero, Polmostundra, Okhmylk and Shongui deposits of the Kola rare-metal pegmatite belt, expressed in terms of (**a**) Nb (apfu) vs. Ta (apfu), (**b**) Mn (apfu) vs. Fe (apfu) and (**c**,**d**) Mn/(Mn + Fe) vs. Ta/(Ta + Nb). CGMs are from the same samples as in Table 1.

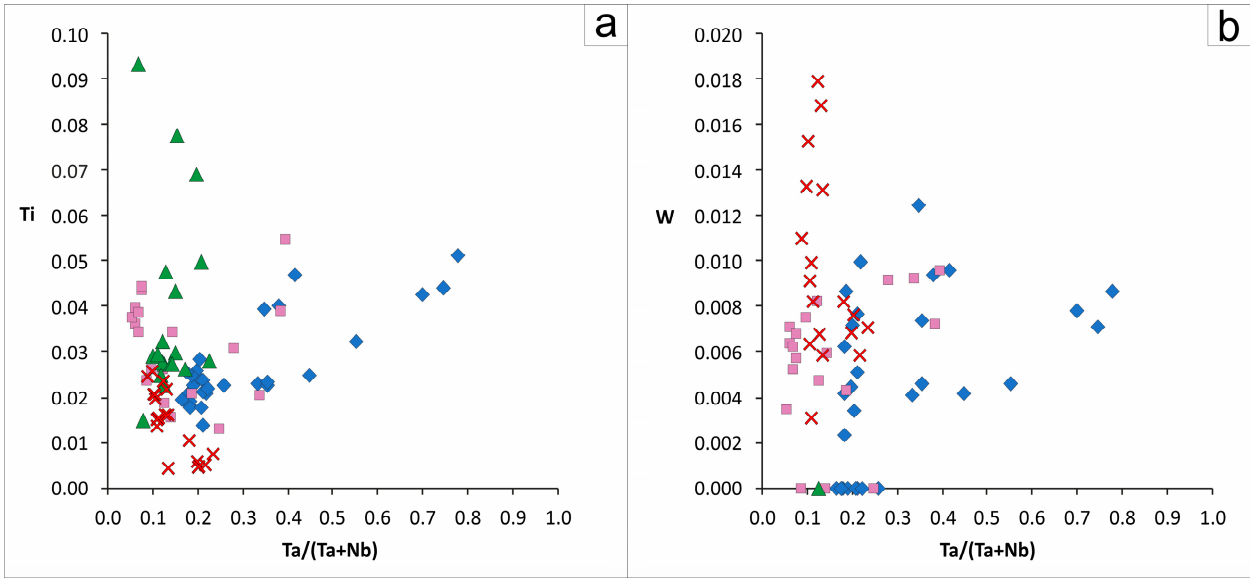


Figure 7. Minor-element compositions in CGM from the Kola rare-metal pegmatite belt expressed in terms of (**a**) Ta/(Ta + Nb) vs. Ti (apfu) and (**b**) Ta/(Ta + Nb) vs. W (apfu). Same symbols as Figure 6.

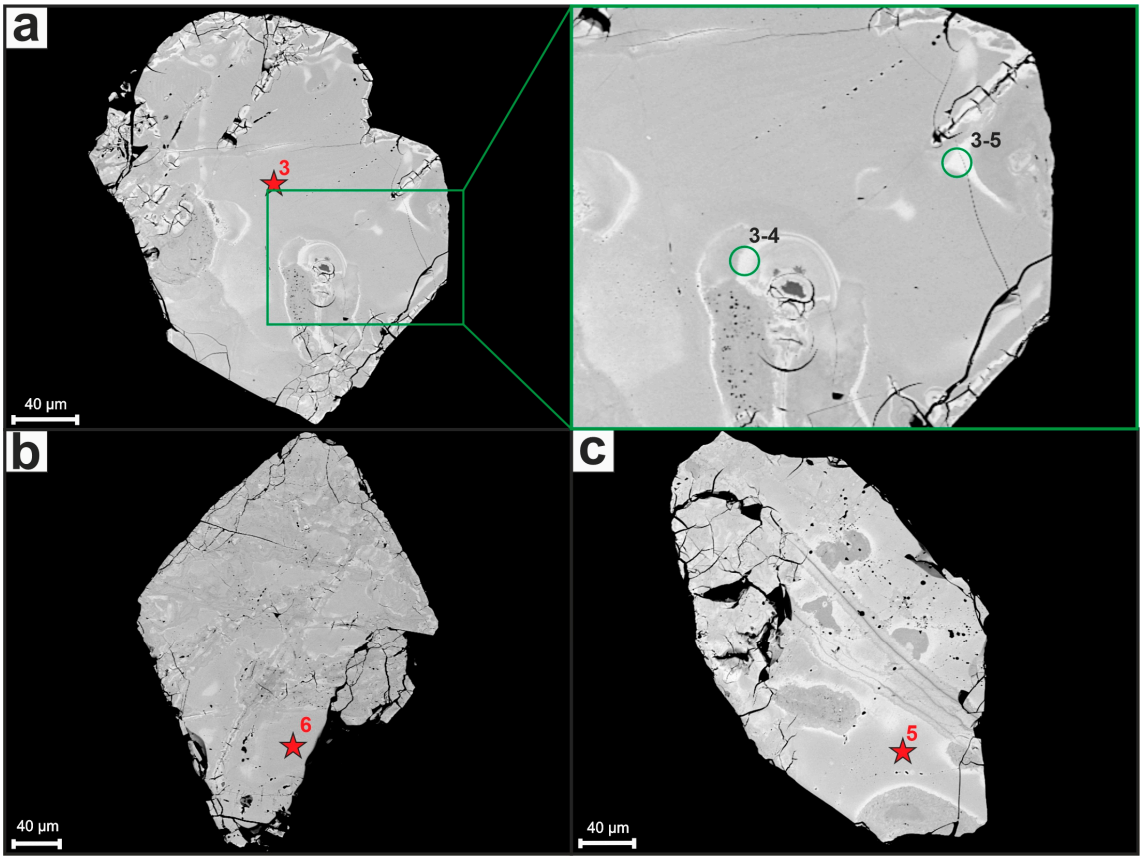


Figure 8. Representative back-scattered electron (BSE) images of PSGM grains from the Polmostudra pegmatites, illustrating the morphology and internal textures. Thin zones with elevated Ta, U and Pb (**a**); euhedral grains with octahedral habit (**b**,**c**). Red stars indicate microprobe analyses, green circles indicate SEM analyses.

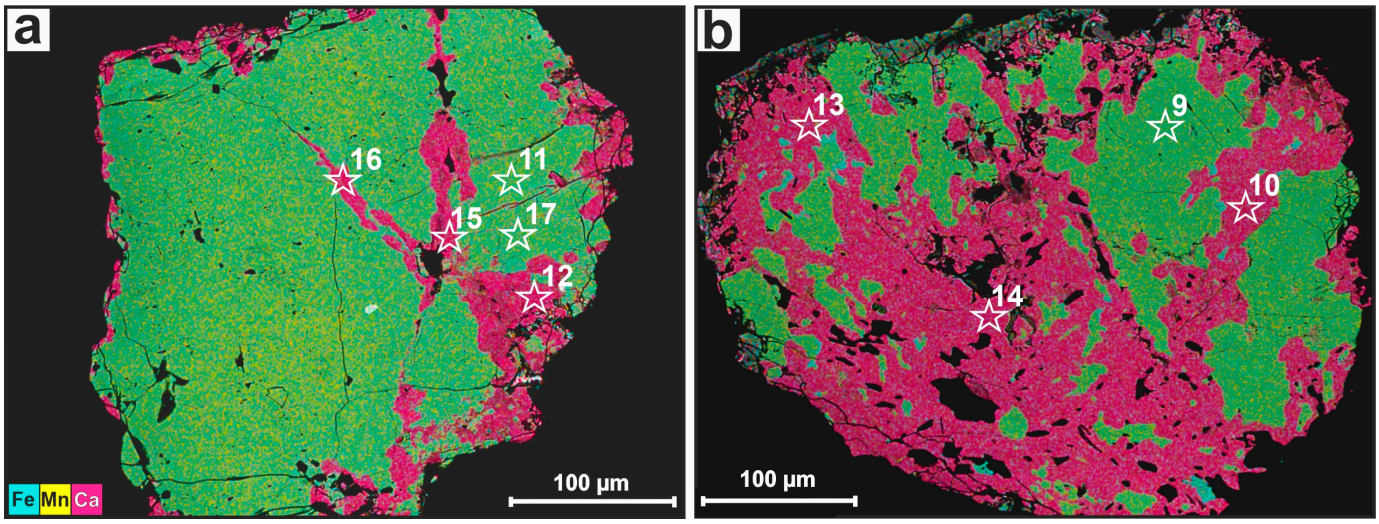


Figure 9. EMPA mapping (Fe, Mn, Ca) of CGM and PSGM, showing the formation of PSGM along the rim and internal fractures in CGM (**a**), and more extensive replacement of CGM by PSGM (**b**). Stars indicate microprobe analyses.

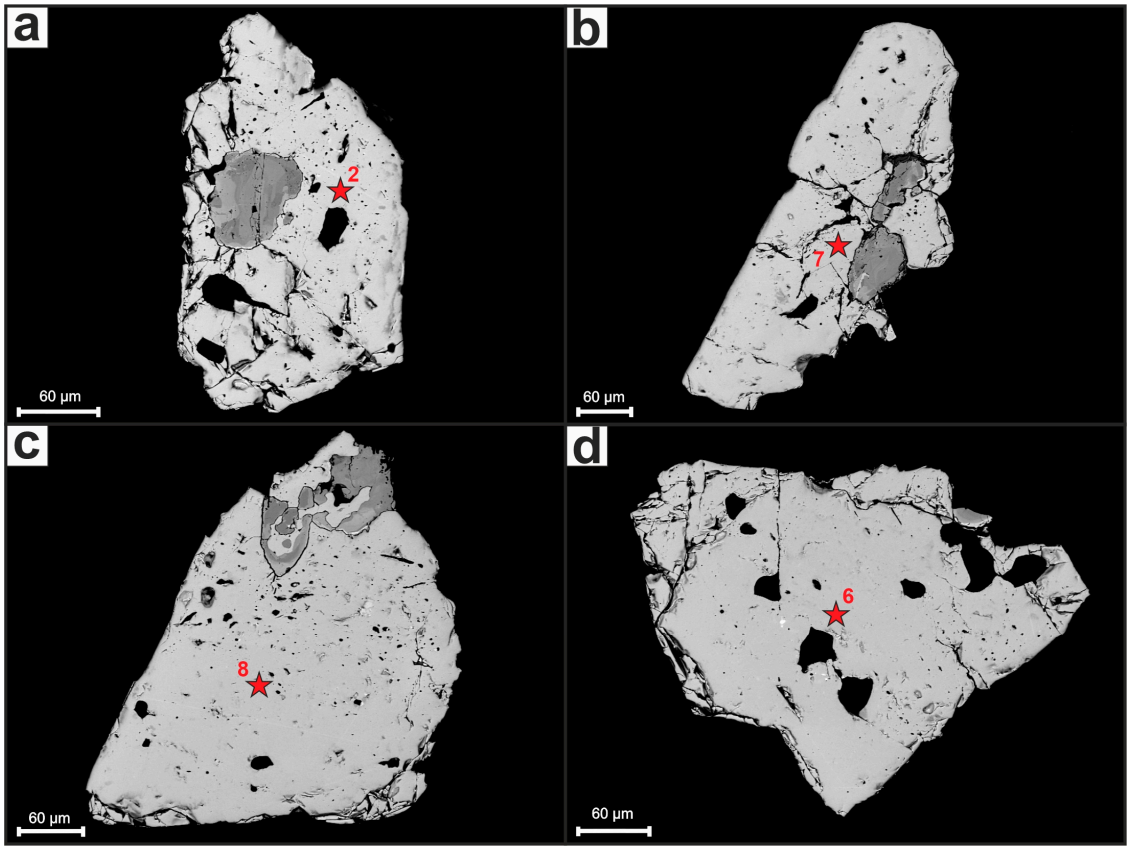


Figure 10. Representative back-scattered electron (BSE) images of cassiterite grains from the Okhmylk pegmatites, showing morphology and internal textures. Inclusions of CGM (**a**–**c**); porous texture and rounded inclusions of quartz and albite (**a**–**d**).

4. Results and Discussion

4.1. Zoning and Mineral Inclusions in CGM

The brightness in the domain being observed in a BSE image of a mineral correlates with the average atomic mass of the elements constituting the domain. The atomic mass of

Ta (≈181 amu) is nearly double that of Nb (≈93), while Mn and Fe have very similar atomic masses (≈55 amu and ≈56 amu, respectively). Thus, the brightest domains in the BSE images of the studied CGM grains have high Ta concentrations, while the dark domains are rich in Nb. Variations in the concentrations of Mn and Fe have much smaller effect on the brightness in BSE images of CGM.

4.1.1. Kolmozero Deposit

The predominant parts of the CGM grains are homogeneous or show oscillatory zoning (sometime concentric), but some grains show irregular patchy compositional patterns (Figure 2). The oscillatory zoning observed for some CGM indicates that the grains crystallized under non-equilibrium conditions during fractional crystallization of the pegmatite melt. This compositional pattern is characteristic of magmatic CGMs from granites and pegmatites worldwide, such as the Shangbao granite [44], the Penouta leucogranite and greisen [16,45], the Separation Lake pegmatite [46], the Tanco pegmatite [11,47], the East-Qinling pegmatite district [9] and the Jezuitské Lesy pegmatite [48]. Niobium and Ta show slow diffusion, relative to the rate of crystal growth in the crystallization front of the pegmatite [11,49–51], which is explained as a process of constitutional zone refining [52]. In contrast, the compositionally homogeneous CGM indicate equilibrium conditions during crystallization, with coexisting silicate melt and a separate fluid phase [53]. Under such conditions, CGM might crystallize directly from the melt.

The patchy pattern, with irregularly distributed and alternating brighter and darker elongated domains (in BSE images) throughout the CGM grains, is typical of late-stage, low-temperature CGM-bearing parageneses in the Kolmozero pegmatite [8]. It has been suggested that the pattern formed during significant changes in the activities of Nb and Ta in the grain boundary fluid. The patchy pattern is somewhat similar to "myrmekitic" and "embayment" textures observed in CGM from the Chakabeishan deposit [17]. It has been suggested that these CGMs were formed by metasomatism and the replacement of early-formed CGM by fluids released from the most evolved melt [46,49]. This is supported by bright overgrowths on early-formed homogeneous CGM grains, as observed in BSE images.

Inclusions observed in the studied Kolmozero CGM include a rectangular grain of Nb-Ta-Ca-Na-oxide (30 × 40 μm, possibly a pyrochlore group mineral), an elongated grain of apatite (80 × 20 μm) and tiny (<1 μm) grains of Pb-rich uraninite, bismuth, bismite, galena and sphalerite.

4.1.2. Polmostundra Deposit

Although most of the CGM from the Polmostundra deposit are homogeneous, some of the grains show similar internal textures, and apparently have the same origin as the Kolmozero CGM (Figure 3). Some of the grains that are homogenous and bright in BSE images are overgrown by darker porous rims. Less abundant are the patchy and mottled CGMs. The patchy grains are similar to the ones from Kolmozero. The mottled (convoluted) texture is characterized by irregularly shaped domains with embayment into each other and gradual variations in shades of gray in the BSE images. It can be observed that the mottled texture overprints an earlier internal oscillatory zoning in grains of CGM (Figure 3a,b). We infer that the mottled texture formed during a late stage in response to changes in the activities of Nb and Ta, in the same way as the patchy pattern. In general, CGM from the Polmostundra deposit often shows reverse zoning, with the formation of late domains that are dark in BSE images. This is not common for CGM from pegmatites, but it has been described in granite and pegmatite (i.e., [45,54]). Uraninite and galena are common mineral inclusions in CGM from the Polmostundra deposit.

4.1.3. Okhmylk Deposit

Almost all studied CGM from Okhmylk shows a patchy pattern in BSE images, but some homogeneous grains are observed (Figure 4). The patchy pattern is represented by two subtypes: (1) the alternation of dark and bright bands (Figure 4c), and (2) irregular

bright domains confined to the rims of the CGM (Figure 4d). The conspicuous feature of the Okhmylk sample is the presence of abundant intergrowths of CGM and Nb-Ta-Ca-(±Ti, Mn)-oxide (possibly a pyrochlore group mineral) (see Section 4.3).

Subhedral Pb-rich uraninite (<6 μm) and zircon (<5 μm) occur as inclusions in CGM from the Okhmylk deposit, which are homogeneous in BSE images.

4.1.4. Shongui Deposit

CGM from the Shongui deposit usually exhibits a zoned texture characterized by dark-gray cores and gray rims in BSE images (Figure 5). Occasionally, this zonation is normal, and the thickness of the rims is similar to the core diameter. In some cases, bright rims form thin discontinuous bands, with a sharp boundary with the main crystal. These bands are inferred as late overgrowths. Some grains show oscillatory zoning, characterized by multiple bright and dark bands in BSE images. Several grains show a complex combination of different types of zoning, such as an inner core with oscillatory zoning enclosed in a homogenous outer zone. These grains have reverse zoning, as the homogeneous outer zones are dark in BSE images. Based on the internal textures of CGM from the Shongui deposit, the following crystallization scheme can be suggested (see previous discussion in Section 4.1.1): (1) formation of oscillatory zoning during the magmatic stage under disequilibrium conditions; (2) crystallization of homogeneous CGM (dark in BSE images) during the magmatic stage; (3) crystallization of homogeneous CGM (bright in BSE images) from evolved melt at a late-magmatic stage; and (4) overgrowth of thin rims of CGM (brightest in BSE images) at a post-magmatic (hydrothermal) stage.

Clusters of small (<10 μm) rounded inclusions of Ta-Nb-Ca-Si-Ti-(±Sn)-O composition (possibly a pyrochlore supergroup mineral) are characteristic features of CGM from the Shongui deposit. These inclusions are confined to the central parts of the host mineral.

4.2. Mineral Chemistry of CGM

The chemical formulae of CGM with the ranges of the sites are the following: $(Fe_{0.39–0.78}$ $Mn_{0.18–0.66}$ $Ti_{0.02–0.05})$ $(Nb_{0.57–1.62}$ $Ta_{0.32–1.45}$ $Si_{0.01–0.08})_2O_6$ for Kolmozero, $(Fe_{0.68–0.89}$ $Mn_{0.12–0.36}$ $Ti_{0.01–0.05}$ $Mg_{0–0.01}$ $Zn_{0–0.01})$ $(Nb_{1.11–1.83}$ $Ta_{0.12–0.73}$ $Si_{0–0.05}$ $Sn_{0–0.02}$ $W_{0–0.01})_2O_6$ for Polmostundra, $(Fe_{0.08–0.74}$ $Mn_{0.30–0.93}$ $Ti_{0–0.03})$ $(Nb_{1.49–1.79}$ $Ta_{0.17–0.46}$ $Si_{0–0.02}$ $W_{0.01–0.02})_2O_6$ for Okhmylk, and $(Fe_{0.46–0.68}$ $Mn_{0.30–0.55}$ $Ti_{0.02–0.08})$ $(Nb_{1.42–1.80}$ $Ta_{0.13–0.41}$ $Si_{0–0.01})_2O_6$ for Shongui. All of the analyzed CGM from the Kolmozero–Voronja pegmatites show negative correlations in the diagrams of Nb vs. Ta and Mn vs. Fe (Figure 6a,b), suggesting the substitution of Ta with Nb and Fe with Mn. The Kolmozero CGM show the highest Ta content, while the CGM from the Okhmylk pegmatites show highest Mn content. The Polmostundra CGM show mainly Nb- and Fe-rich compositions. Compositions and element ratios of the analyzed CGM are shown in the columbite quadrilateral diagrams (Figure 6c,d). Most of the compositions plot within the columbite-(Fe) and columbite-(Mn) fields, with single points of tantalite-(Fe), tantalite-(Mn) and species close to tapiolite-(Fe). The minerals from the four studied deposits may have variable overall contents in both major (Nb, Ta, Fe, Mn) and essential minor (Ti, W, Sn, Zr, Si) components. CGM from Li pegmatites (Kolmozero, Polmostundra, and Okhmylk) have impurities of Ti (0.01–0.05 apfu) and W (0.002–0.018 apfu), whereas mineral from Be pegmatites (Shongui) contains elevated Ti (0.02–0.09 apfu) and W below the detection limit (Figure 7).

4.2.1. Kolmozero Deposit

Ta/(Ta + Nb) and Mn/(Mn + Fe) ratios in Kolmozero CGM vary, and are within 0.16–0.70 and 0.45–0.63, respectively. Most of the homogeneous CGM and CGM with oscillatory zoning are classified as columbite-(Fe), or, more rarely, as columbite-(Mn). Most of the patchy domains in CGM are classified as tantalite-(Fe) and columbite-(Mn), and, rarely, as columbite-(Fe). Rims and domains interpreted as late overgrowths are classified as tantalite-(Fe). Some homogeneous grains of tantalite-(Mn) show a 'sponge-like' texture; i.e., they contain numerous tiny pores (Figure 2d). Similar textures have been related to overprinting processes resulting

from the influx of hydrothermal fluids (e.g., [45,55–57]). For the Kolmozero pegmatites, columbite-tantalite shows variations along two compositional trends: from columbite-(Fe) to tantalite-(Fe), and from columbite-(Fe) to columbite-(Mn) (±tantalite-(Mn)). This suggests a significant increase in fluorine activity during crystallization, due to intensive fractionation of the pegmatite-forming melt-fluid system [19,20]. CGMs from the Kolmozero deposit show low concentrations of TiO_2 (0.29–0.89 wt.%, average 0.54 wt.%), WO_3 (0–0.61 wt.%, average 0.32 wt.%) and SiO_2 (0.17–1.40 wt.%, average 0.39 wt.%), whereas Sn and Zr are below the detection limit. High TiO_2 concentrations are observed in CGM, with elevated Ta/(Ta + Nb). Patchy and porous CGM contains ZnO, ranging from 0.07 to 0.20 wt.%.

4.2.2. Polmostundra Deposit

The CGMs from Polmostundra show compositions in the columbite-(Fe) field, see Figure 5c. The Mn/(Mn + Fe) ratio varies between 0.12 and 0.33, and the Ta/(Ta + Nb) ratio between 0.05 and 0.39. The mineral shows a tendency for increasing Ta/(Ta + Nb) and, to some extent, for Mn/(Mn + Fe), from the homogeneous and oscillatory grains toward the patchy ones and rim overgrowths. CGMs in dark zones in BSE images with reverse zoning and embayments cutting into the oscillatory and homogeneous cores show the lowest Ta/(Ta + Nb), in the range 0.05–0.07. The compositional variations of Nb and Ta suggest a complicated scheme for crystallization of CGM in the Polmostundra pegmatite; i.e., (1) Ta enrichment during magmatic fractionation (evidence from oscillatory and homogeneous CGM), (2) consumption of Ta in the system, due to the formation of other Ta-bearing minerals toward the end of the magmatic stage (outer zones in reverse CGM and embayments on mottled CGM), and (3) crystallization of high-Ta CGM during a hydrothermal stage (bright domains in patchy CGM, overgrowing rims and domains). Minor components show highly variable concentrations: TiO_2 (0.27–1.07 wt.%, average 0.69 wt.%), WO_3 (0–0.54 wt.%, average 0.35 wt.%), SiO_2 (0–0.69 wt.%, average 0.22 wt.%), SnO_2 (0–0.84 wt.%, average 0.10 wt.%), and ZnO (0–0.16 wt.%, average 0.06 wt.%). The highest W, Zn and Sn contents are observed in the latest CGM, showing high Ta/(Ta + Nb) ratios (bright domains in patchy CGM, overgrowing rims and domains).

4.2.3. Okhmylk Deposit

CGMs from the Okhmylk deposit show compositions corresponding to columbite-(Fe) and columbite-(Mn) in Figure 6d, with Mn/(Mn + Fe) ratios ranging between 0.29 and 0.92, and Ta/(Ta + Nb) between 0.09 and 0.24. Some analyses with high Ta/(Ta + Nb) also show high Mn/(Mn + Fe). The highest Mn/(Mn + Fe) are detected in patchy domains (both in BSE dark and bright domains). Homogeneous CGM and minerals with normal compositional zoning show lowest Mn/(Mn + Fe) ratios. This indicates that the enhanced Mn/(Mn + Fe) ratios result from reactions with a late-stage hydrothermal fluid, rather than during fractional crystallization (e.g., [8,11,58]). Another factor controlling the Fe-Mn fractionation in CGM is competitive crystallization of paragenetic Fe-bearing minerals (i.e., tourmaline, mica and Fe-oxides) and of Mn-bearing minerals (i.e., apatite, spessartine and triphylite-lithiophilite phosphates; see [9,59]). Abundant tourmaline (mainly schorl), together with accessory magnetite in the Okhmylk sample (see Table 1), are considered to be responsible for an increase in the Mn content of the late-stage pegmatitic melt during the continuous crystallization of CGM.

The CGM from the Okhmylk deposit differs from CGM from the other pegmatites studied here, in its low TiO_2 (0.09–0.58 wt.%, average 0.33 wt.%), high WO_3 (0.20–1.15 wt.%, average 0.61 wt.%), detectable Sc_2O_3 (0.08–0.23 wt.%, average 0.15 wt.%), and SnO_2 and ZnO below their detection limits. The minor-element contents result both from melt evolution and the mineral assemblage for the Okhmylk CGM. Tungsten and Ti, as incompatible elements, prefer to enter the residual melt during magmatic evolution. Scandium is a compatible element, and prefers to enter mafic minerals, such as pyroxene and amphibole. In general, pegmatites show low concentrations of Sc, but in F-enriched melts, Sc can be significantly enriched in the residual melt during magmatic evolution, due to the high

chemical affinity of Sc to F [60]. The absence of tin in CGM is apparently controlled by abundant cassiterite in the Okhmylk pegmatite (see Section 4.3, below).

4.2.4. Shongui Deposit

The predominant CGM from the Shongui sample is columbite-(Fe), with the two exceptions of columbite-(Mn). The CGM show Ta/(Ta + Nb) ratios ranging from 0.07 to 0.23 (average 0.14) and Mn/(Mn + Fe) ratios from 0.31 to 0.55 (average 0.4). Columbite-(Mn) occurs in cores that are dark in BSE images [Ta/(Ta + Nb) = 0.08] and in overgrowths that are bright in BSE images [Ta/(Ta + Nb) = 0.23]. The normal zoning (dark core and bright rim in BSE images) mainly reflects an increase in Ta content toward the rims. Grains with oscillatory zoning are characterized by Ta/(Ta + Nb) ratios in the range 0.15–0.2 and Mn/(Mn + Fe) ratios in the range 0.33–0.44. It may be concluded that the Nb-Ta fractionation in CGM from Shongui is mainly controlled by magmatic differentiation (both equilibrium and non-equilibrium), while hydrothermal processes (represented by rare Ta-rich overgrowing rims) are suppressed.

CGMs from the Shongui deposit are characterized by minor-element contents which are different from the other pegmatites reported here. TiO_2 ranges from 0.34 to 2.12 wt.% (average 0.84 wt.%), whereas Zr, W, Sc, Sn and Zn are negligible or below their detection limits. The highest TiO_2 content was detected in CGM with oscillatory zoning (1.5–1.7 wt.%) and in cores of grains with normal zoning (0.6–2.12 wt.%), i.e., in minerals formed during an early magmatic stage.

4.3. Associated Pyrochlore Supergroup Minerals and Cassiterite

Pyrochlore supergroup minerals (PSGMs) are identified in samples from the Polmostundra, Okhmylk and Shongui pegmatites. PSGMs are abundant in Polmostundra, where they form individual grains. For the Okhmylk pegmatite, PSGMs occur as overgrowths on CGM, while for the Shongui pegmatite, PSGM grains occur as tiny inclusions in CGM.

PSGMs from *Polmostundra* form subhedral and anhedral 200–300 μm grains (Figure 8), with an inhomogeneous internal texture characterized by irregularly distributed thin zones that are bright in BSE images (due to high Ta, U and Pb, see Table 3). Mineral compositions are given in Table 3. The B site is mainly occupied by Ta (1.835–1.917 apfu) and, to a lesser extent, by Nb (0.052–0.111 apfu), W (0.016–0.028 apfu) and Sn (0–0.043 apfu), with Fe, Ti, Al and Mg below their detection limits. The A site is almost completely occupied by Na (0.825 to 0.986 apfu) and Ca (0.6 to 0.863 apfu), with varying contents of U (0–0.155 apfu) and Sr (0.049–0.144 apfu). The contents of Mn, Pb and Th are insignificant or below the detection limits. PSGMs show variable contents of F and OH, and classify as fluoronatromicrolite/hydroxynatromicrolite, with an average formula $(Na_{0.90}\ Ca_{0.74}\ Sr_{0.08}\ U_{0.07}\ Pb_{0.03}\ Mn_{0.01})_{1.84}\ (Ta_{1.87}\ Nb_{0.09}\ Sn_{0.02}\ W_{0.02})_2\ (F_{0.55}\ OH_{0.45})$. Microlite is the only Nb-Ta oxide from the studied pegmatite showing a significant content of uranium (1.02 to 7.24 wt.%, average 3.85 wt.%, of UO_2), suggesting that it formed during the replacement of early-formed Nb–Ta minerals (see [12,61]). Accordingly, the microlite shows the highest Ta/(Ta + Nb) ratio (0.94–0.97) of all of the Nb and Ta oxides of the studied pegmatites, supporting its evolved character. Most analyses show fluorine > 0.5 apfu; however, U-enriched microlite contains up to 0.5 apfu OH. Fluorine is below the detection limit in the thin zones, with elevated Pb and U. High Pb content in microlite is partly related to secondary alteration [14]. Thus, it can be suggested that microlite crystallized during a late metasomatic/hydrothermal stage during pegmatite formation.

Okhmylk PSGM formed during the replacement of columbite-(Mn). Columbite-(Mn), which formed during a magmatic stage, was initially homogeneous. The alteration of columbite-(Mn) started along the rim and internal fractures (Figure 9a), and progressed until the mineral was partly or completely altered, to PSGM (Figure 9b). The PSGM from Okhmylk is classified as hydroxycalciopyrochlore, with the average formula $(Ca_{1.00}\ Mn_{0.07}\ Fe_{0.01}\ Y_{0.01})_{1.08}\ (Nb_{1.76}\ Ta_{0.23}\ Ti_{0.01})_2\ (OH_{1.00})$. For all analyses, the contents of Na and F are below their detection limits. The mineral shows elevated Y_2O_3 content (0.28–0.44 wt.%)

and high vacancies in the A site (0.62–0.99 apfu). Pyrochlore and primary columbite show similar Ta/(Ta + Nb) ratios. The Mn/(Mn + Fe) ratio is exceptionally high in pyrochlore, compared to columbite (0.68–1.0 and 0.57–0.67, respectively). The replacement process was probably driven by Ca-rich hydrothermal solutions. During the alteration, both Nb and Ta appear to have been immobile. The Mn-Fe substitution series shows the fractionation with the removal of iron.

An estimate of the average composition of *PSGM* from *Schongui* (see Figure 5d) suggests that the mineral is hydroxycalciomicrolite, with the formula $(Ca_{1.13}\ Na_{0.12}\ As_{0.07}\ Fe_{0.06}\ Mn_{0.03}\ U_{0.02})_{1.42}\ (Ta_{0.91}\ Si_{0.65}\ Nb_{0.37}\ Sn_{0.04}\ Mg_{0.01}\ Al_{0.01})_2\ (OH_{1.00})$. The average Ta/(Ta + Nb) and Mn/(Mn + Fe) are 0.72 and 0.38, respectively. The host mineral is columbite-(Fe) or, less commonly, columbite-(Mn), with Ta/(Ta + Nb) and Mn/(Mn + Fe) ratios in the range 0.08–0.17 and 0.41–0.54, respectively.

Cassiterite was recovered only from the Okhmylk pegmatite. The mineral occurs as anhedral and subhedral angular grains (200–300 μm) (Figure 10). The internal texture is inhomogeneous, due to the presence of porous domains. Cassiterite grains often contain inclusions (20–40 μm) of albite and, rarely, quartz, resembling a poikilitic texture. These textural patterns are different from those observed in cassiterites forming at magmatic stages of pegmatite formation (i.e., homogeneous, without pores and inclusions of late minerals, see [46,58,62]). Cassiterite contains inclusions of rounded and partially resorbed CGM (40–60 μm). The CGMs are of both magmatic (normal compositional zoning) and metasomatic/hydrothermal (with patchy domains) types. Cassiterite, enclosing magmatic CGM, has been reported in a number of pegmatite occurrences, i.e., the Separation Rapids in Canada [46] and Kangxiwa–Dahongliutan in China [58]. The chemical composition of cassiterite from Okhmylk is near ideal SnO_2 (the majority of the grains have >99 wt.% SnO_2), with variable contents of trace elements (Fe: 0–0.012, average 0.003 apfu; Nb: 0–0.007, average 0.002 apfu; Ta: 0–0.027, average 0.007 apfu; Mn, Mg, Zr, and Ti are below their detection limits). The compositions are typical for cassiterite from a hydrothermal environment [62].

4.4. Implication for Ore Genesis and Grade

Nb-Ta-Sn oxides (among which, the columbite group minerals, the pyrochlore supergroup minerals and cassiterite are the most common), can provide information about the formation of LCT-pegmatites of different ore grades and mineralization signatures. Variations in the composition and internal textures of Nb-Ta-Sn oxides are mainly controlled by the rate of magmatic fractionation, mineral associations of the host pegmatite, the composition of the magmatic fluid, and later hydrothermal/metasomatic processes. As a result of fractional crystallization, the composition of CGM generally shows a continuum from early Nb-rich to later Ta-rich compositions [63,64]. Normal and oscillatory zoning, homogeneous compositions are of magmatic origin, and controlled by Nb-Ta fractionation. Previous studies have proved that the patchy and mottled textures of CGM, as well as the overgrowing Ta-rich rims, are generally related to metasomatic replacement during reactions with hydrothermal fluids (e.g., [8,11,58]). Fractionation of Fe and Mn, which is difficult to relate to any of the processes mentioned above, was probably controlled by the mineral associations during crystallization. Reverse zoning is rarely observed in CGM from rare-metal pegmatites, and may be attributed to local changes in the bulk geochemistry and/or fluid regime of the pegmatite.

The main compositional and textural features of Nb-Ta-Sn oxides from the studied pegmatite samples from the Kolmozero–Voronja belt are summarized in Table 5.

Table 5. Summary of mineralogical features of Nb-Ta-Sn oxides from pegmatite samples in Kolmozero–Voronja pegmatite belt.

Deposit/Occurrence	**Kolmozero**	**Polmostundra**	**Okhmylk**	**Shongui**
Sample N	**KL-GX-11**	**POL-GX-3/5**	**OKH-2/2**	**SH-7**
Mineralization signature	Li (±Nb, Ta)	Li-Cs (±Nb, Ta)	Li (±Nb, Ta)	Be (±Nb, Ta)
Ore grade (based on Li content)	High	Medium to low	Low to barren	Low to barren
CGM	columbite-(Fe) columbite-(Mn) tantalite-(Fe) tantalite-(Mn)	columbite-(Fe)	columbite-(Fe) columbite-(Mn)	columbite-(Fe) columbite-(Mn)
Texture/zoning/pattern (in descending order)	oscillatory homogeneous patchy sponge domains overgrowing Ta-rich rims	homogeneous mottled oscillatory patchy irregular reverse	irregular normal patchy homogeneous	progressive normal oscillatory homogeneous irregular reverse overgrowing Ta-rich rims
Overall composition features:				
Ta/(Ta + Nb)	0.16–0.70	0.05–0.39	0.09–0.24	0.07–0.23
Mn/(Mn + Fe)	0.45–0.63	0.12–0.33	0.29–0.92	0.31–0.55
Ti (apfu)	0.01–0.05	0.01–0.05	0–0.025	0.02–0.09
W (apfu)	0.002–0.012	0.0–0.009	0.003–0.018	0.0
PSGM	calciopyrochlore (included in columbite-(Fe))	fluoronatromicrolite (abundant individual grains of hydrothermal origin)	hydroxycalciopyrochlore (replaced columbite-(Mn))	hydroxycalciomicrolite (included in columbite-(Fe))
Cassiterite	No (0–0.5 wt.% of SnO_2 in CGM)	No (0–0.84 wt.% of SnO_2 in CGM)	abundant porous grains of hydrothermal origin (0.0 wt.% of SnO_2 in CGM)	No (0–0.2 wt.% of SnO_2 in CGM)
Main evolution trends for Nb-Ta-Sn oxides:	Calciopyrochlore → columbite-(Fe) → columbite-(Mn); columbite-(Fe) → tantalite-(Fe)/tantalite-(Mn).	Columbite-(Fe) → columbite-(Fe) with higher Ta/(Ta + Nb) → fluornatromicrolite → hydroxynatromicrolite with high Ta, U and Pb content.	Columbite-(Fe)/columbite-(Mn) → hydroxycalciopy-rochlore → cassiterite.	Hydroxycalciomicrolite → columbite-(Fe) → columbite-(Fe) with higher Ta/(Ta + Nb).

Based on the information given in Table 5, we infer that both magmatic and hydrothermal processes controlled the Nb-Ta and Fe-Mn fractionation of CGM from the high-grade Kolmozero Li deposit. For the medium- to low-grade Polmostundra Li (±Cs) deposit, magmatic processes were less pronounced for Nb-Ta fractionation of the CGM, while hydrothermal processes were important during the crystallization of microlite. For the low-grade Okhmylk Li deposit, we infer that Nb-Ta fractionation was insignificant for CGM during the magmatic stage. However, the fractionation of Fe and Mn controlled by the mineral association, i.e., the crystallization of Fe minerals (schorl) was significant in Okhmylk CGM. Hydroxycalciopyrochlore and cassiterite are of hydrothermal origin. For the CGM from the low-grade Shongui Be (±Ta) deposit, any Nb-Ta fractionation during the magmatic stage is considered to be insignificant. The hydroxycalcio-species of PSGM crystallized during an early magmatic stage, while the fluoronitro-species formed in a

hydrothermal environment, probably during reactions with sodium and fluorine in excess in late-stage hydrothermal solutions.

Late tantalum-rich Nb-Ta oxides (CGM and PSGM from Kolmozero and Polmostundra) have an elevated Sn content that is in accordance with presumable partitioning of tin into late-stage hydrothermal phases [65]. The consumption of Sn by abundant CGM from these deposits did not allow cassiterite precipitation. The opposite can be inferred for the niobium-rich CGM and PSGM from Okhmylk, which do not contain Sn. Here, Sn was allowed to accumulate in the late fluid phase, resulting in the crystallization of hydrothermal cassiterite.

The petrogenetic processes that were active during the formation of the high-grade Kolmozero deposit resulted in the crystallization of abundant CGM, showing large compositional variations. Volatile components may have played an important role in the rare-metal enrichment. Indeed, the Kolmozero sample has an elevated concentration of CO_2 (0.25 wt.% vs. <0.01–0.02 wt.% in low-grade samples (see Table 1)). Due to the strong depolymerization effect of CO_2, a high CO_2 content causes rapid separation of volatile-rich melts from the initial magma, through immiscibility [66]. At this stage, the activity of rare metals increased. Furthermore, CO_2 is exhausted earlier than other volatiles, promoting extensive hydrothermal processes and rare-metal precipitation, in response to pressure and temperature drop and/or pH change [67].

5. Conclusions

1. CGM from high-grade Li pegmatite deposits from the Kolmozero–Voronja belt are characterized by several mineral species showing large variations in chemical compositions, mainly controlled by Nb-Ta fractionation. Textural patterns are extremely various (oscillatory, homogeneous, patchy, and mottled), and indicate the involvement of numerous magmatic and hydrothermal processes.
2. Nb-Ta magmatic fractionation in CGM from low-grade and barren pegmatite deposits is insignificant.
3. Fe-Mn fractionation is mainly controlled by precipitation of certain Fe minerals during pegmatite formation, and does not play an important role in the grade of the deposits.
4. PSGM from high- to medium-grade lithium deposits are magmatic (Nb varieties) and early hydrothermal (Ta varieties), while in low-grade-to-barren pegmatites, the mineral crystallized at late hydrothermal stages (both Nb and Ta varieties). PSGM from beryllium deposits are early magmatic Ta varieties, and crystallized before CGM.
5. Sn is concentrated in CGM from high- to medium-grade Li pegmatites, while it forms abundant hydrothermal cassiterite in low-grade and barren pegmatites.
6. Be-Ta pegmatites from the Kolmozero–Voronja belt are characterized by CGM with the lowest variations in fractionation ratios Ta/(Ta + Nb) and Mn/(Mn + Fe) and highest Ti contents.

Supplementary Materials: The following supporting information can be downloaded at: https://www.mdpi.com/article/10.3390/geosciences14010009/s1, Table S1: Whole data set of Nb-Ta-Sn oxides.

Author Contributions: Conceptualization, D.Z. and L.N.M.; methodology, A.B.; formal analysis, K.K.; investigation, D.Z.; resources, L.N.M.; writing—original draft preparation, D.Z.; writing—review and editing, K.K.; visualization, D.Z. All authors have read and agreed to the published version of the manuscript.

Funding: Russian Science Foundation Grant No. 22-17-20002, https://rscf.ru/project/22-17-20002/ (accessed on 25 March 2022).

Data Availability Statement: Data are contained within the article and Supplementary Materials.

Acknowledgments: We thank S. Mudruk and A. Solovjeva, who assisted with drawing, and T. Zikova for Nb-Ta-Sn oxide separation. The manuscript was much improved through constructive criticism from three anonymous reviewers, who are gratefully acknowledged.

Conflicts of Interest: The authors declare no conflict of interest.

References

1. Černý, P.; Ercit, T.S. Some recent advances in the mineralogy and geochemistry of Nb and Ta in rare-element granitic pegmatites. *Bull. Mineral.* **1985**, *108*, 499–532. [CrossRef]
2. Černý, P.; Ercit, T.S. Mineralogy of niobium and tantalum: Crystal chemical relationships., paragenetic aspects and their economic implications. In *Lanthanides, Tantalum and Niobium*; Moller, P., Cerny, P., Saupe, F., Eds.; Springer: Berlin/Heidelberg, Germany, 1989; pp. 27–79.
3. Raimbault, L. Composition of complex lepidolite-type granitic pegmatites and of constituent columbite-tantalite, Chedeville, Massif Central, France. *Can. Mineral.* **1998**, *36*, 563–583.
4. Uher, P.; Černý, P.; Chapman, R.; Hatar, J.; Miko, O. Evolution of Nb. Ta-oxide minerals in the Prasiva granitic pegmatites, Slovakia; I, Primary Fe, Ti-rich assemblage. *Can. Mineral.* **1998**, *36*, 525–534.
5. Lumpkin, G.R. Composition and Structural State of Columbite—Tantalite from the Harding Pegmatite, Taos Countv, New Mexico. *Can. Mineral.* **1998**, *36*, 585–599.
6. Novák, M.; Uher, P.; Černý, P.; Siman, P. Compositional variations in ferrotapiolite+tantalite pairs from the beryl-columbite pegmatite at Moravany nad Váhom, Slovakia. *Mineral. Petrol.* **2000**, *69*, 295–306.
7. Beurlen, H.; Da Silva, M.R.R.; Thomas, R.; Soares, D.R.; Olivier, P. Nb-Ta-(Ti-Sn) oxide mineral chemistry as tracer of rare-element granitic pegmatite fractionation in the Borborema Province, Northeastern Brazil. *Miner. Depos.* **2008**, *43*, 207–228. [CrossRef]
8. Badanina, E.V.; Sitnikova, M.A.; Gordienko, V.V.; Melcher, F.; Gäbler, H.E.; Lodziak, J.; Syritso, L.F. Mineral chemistry of columbite-tantalite fromspodumene pegmatites of Kolmozero, Kola Peninsula (Russia). *Ore Geol. Rev.* **2015**, *64*, 720–735. [CrossRef]
9. Zhou, Q.; Qin, K.; Tang, D. Mineralogy of columbite-group minerals from the rare-element pegmatite dykes in the East-Qinling orogen, central China: Implications for formation times and ore genesis. *J. Asian Earth Sci.* **2021**, *218*, 104879. [CrossRef]
10. Zhang, A.C.; Wang, R.C.; Hu, H.; Zhang, H.; Zhu, J.C.; Chen, X.M. Chemical evolution of Nb-Ta oxides and zircon from the Koktokay No. 3 granitic pegmatite, Altai, northwestern China. *Mineral. Mag.* **2004**, *68*, 739–756. [CrossRef]
11. Van Lichtervelde, M.; Salvi, S.; Beziat, D.; Linnen, R.L. Textural features and chemical evolution in tantalum oxides: Magmatic versus hydrothermal origins for Ta mineralization in the Tanco Lower Pegmatite, Manitoba. *Can. Econ. Geol.* **2007**, *102*, 257–276. [CrossRef]
12. Llorens, T.; Moro, M.C. Microlite and Tantalite in the LCT Granitic Pegmatites of La Canalita, Navasfrías Sn–W District, Salamanca, Spain. *Can. Mineral.* **2010**, *48*, 375–390. [CrossRef]
13. Martins, T.; Lima, A.; Simmons, W.B.; Falster, A.U.; Noronha, F. Geochemical fractionation of Nb-Ta oxides in Li-bearing pegmatites from the Barroso-Alvão pegmatite field, northern Portugal. *Can. Mineral.* **2011**, *49*, 777–791. [CrossRef]
14. Melcher, F.; Graupner, T.; Gäbler, H.-E.; Sitnikova, M.; Henjes-Kunst, F.; Oberthür, T.; Gerdes, A.; Dewaele, S. Tantalum–(niobium–tin) mineralisation in African pegmatites and rare metal granites: Constraints from Ta–Nb oxide mineralogy, geochemistry and U–Pb geochronology. *Ore Geol. Rev.* **2015**, *64*, 667–719. [CrossRef]
15. Melcher, F.; Graupner, T.; Gäbler, H.-E.; Sitnikova, M.; Oberthür, T.; Gerdes, A.; Badanina, E.; Chudy, T. Mineralogical and chemical evolution of tantalum–(niobium–tin) mineralisation in pegmatites and granites. Part 2: Worldwide examples (excluding Africa) and an overview of global metallogenetic patterns. *Ore Geol. Rev.* **2017**, *89*, 946–987. [CrossRef]
16. González, T.L.; Polonio, F.G.; Moro, F.J.L.; Fernández, A.F.; Contreras, J.L.S.; Benito, M.C.M. Tin-tantalum-niobium mineralization in the Penouta deposit (NW Spain): Textural features and mineral chemistry to unravel the genesis and evolution of cassiterite and columbite group minerals in a peraluminous system. *Ore Geol. Rev.* **2017**, *81*, 79–95. [CrossRef]
17. Sun, W.; Zhao, Z.; Mo, X.; Wei, C.; Dong, G.; Li, X.; Yuan, W.; Wang, T.; Yang, S.; Wang, B.; et al. Age and Composition of Columbite-Tantalite Group Minerals in the Spodumene Pegmatite from the Chakabeishan Deposit, Northern Tibetan Plateau and Their Implications. *Minerals* **2023**, *13*, 201. [CrossRef]
18. Černý, P. Characteristics of pegmatite deposits of tantalum. In *Lanthanides, Tantalum and Niobium*; Möller, P., Černý, P., Saupé, F., Eds.; Springer: Berlin/Heidelberg, Germany, 1989; pp. 195–239.
19. Spilde, M.N.; Shearer, C.K. A comparison of tantalum—Niobium oxide assemblages in two mineralogically distinct rare-element granitic pegmatites, Black Hills, South Dakota. *Can. Mineral.* **1992**, *30*, 719–737.
20. Černý, P.; Němec, D. Pristine vs. contaminated trends in Nb,Ta-oxide minerals of the Jihlava pegmatite district, Czech Republic. *Mineral. Petrol.* **1995**, *55*, 117–129. [CrossRef]
21. Linnen, R.L.; van Lichtervelde, M.; Černý, P. Granitic pegmatites as sources of strategic metals. *Elements* **2012**, *8*, 275–280. [CrossRef]
22. Mitrofanov, F.P.; Lebedev, A.V. (Eds.) *Multimedia Reference Book on Mineral Resources and the Mining Complex of the Murmansk Region: A Digital Information Resource*; GI KSC RAS: Apatity, Russia, 2001. (In Russian)
23. Mints, M.V.; Dokukina, K.A.; Filippova, I.B.; Konilov, A.N. *East European Craton: Early Precambrian History and 3D Models of the Deep Structure of the Earth's Crust*; Geological Society of America (GSA): Boulder, CO, USA, 2015; 433p.
24. Daly, J.S.; Balagansky, V.V.; Timmerman, M.J.; Whitehouse, M.J. The Lapland-Kola Orogen: Palaeoproterozoic collision and accretion of the northern Fennoscandian lithosphere. In *European Lithosphere Dynamics*; Memoir, 32; Gee, D.G., Stephenson, R.A., Eds.; Geological Society: London, UK, 2006; pp. 579–597.
25. Belolipetsky, A.P.; Gaskelberg, V.G.; Gaskelberg, L.A.; Antonyuk, E.S.; Ilyin, Y.U.I. *Geology and Geochemistry of Metamorphic Complexes of the Early Precambrian of the Kola Peninsula*; Nauka: Leningrad, Russia, 1980; 240p. (In Russian)

26. Vrevsky, A.B. *Petrology and Geodynamic Modes of Development of the Archean Lithosphere (on the Example of the Northeastern Part of the Baltic Shield)*; Nauka: Leningrad, Russia, 1989; 143p. (In Russian)
27. Glebovitsky, V.A. *Early Precambrian of the Baltic Shield*; Nauka: St. Petersburg, Russia, 2005; 711p. (In Russian)
28. Hölttä, P.; Balagansky, V.; Garde, A.A.; Mertanen, S.; Peltonen, P.; Slabunov, A.; Sorjonen-Ward, P.; Whitehouse, M. Archean of Greenland and Fennoscandia. *Episodes* **2008**, *31*, 13–19. [CrossRef]
29. McCaffrey, K.J.W.; Lonergan, L.; Wilkinson, J.J. Fractures. In *Fluid Flow and Mineralization*; Geological Society of London: London, UK, 1999; 337p.
30. Morozova, L.N. Kolmozero lithium deposit of rare metal pegmatites: New data on rare element composition (Kola Peninsula). *Lithosphere* **2018**, *18*, 82–98. [CrossRef]
31. Morozova, L.N.; Bazai, A.V. Spodumene from rare-metal pegmatites of the Kolmozerskoe lithium deposit (Kola Peninsula). *Proc. Russ. Mineral. Soc.* **2019**, *148*, 65–78. (In Russian)
32. Morozova, L.N.; Sokolova, E.N.; Smirnov, S.Z.; Balagansky, V.V.; Bazai, A.V. Spodumene from rare-metal pegmatites of the Kolmozero lithium world-class deposit on the Fennoscandian shield: Trace elements and crystal-rich fluid inclusions. *Mineral. Mag.* **2021**, *85*, 149–160. [CrossRef]
33. Zozulya, D.; Macdonald, R.; Bagiński, B. REE fractionation during crystallization and alteration of fergusonite-(Y) from Zr-REE-Nb-rich late- to post-magmatic products of the Keivy alkali granite complex, NW Russia. *Ore Geol. Rev.* **2020**, *125*, 103693. [CrossRef]
34. Gordienko, V.V. *Mineralogy, Geochemistry and Genesis of Spodumene Pegmatites*; Nedra: Leningrad, Russia, 1970; 239p. (In Russian)
35. Morozova, L.N.; Bayanova, T.B.; Bazai, A.V.; Lyalina, L.M.; Serov, P.A.; Borisenko, E.S.; Kunakkuzin, E.L. Rare-metal pegmatites of the Kolmozerskoe lithium deposit in the Arctic region of the Baltic Shield: New geochronological data. *Bull. Kola Sci. Cent. Russ. Acad. Sci.* **2017**, *1*, 43–52. (In Russian)
36. Hanski, E.J.; Melezhik, V.A. Litho- and chronostratigraphy of the Palaeoproterozoic Karelian formations. In *Reading the Archive of Earth's Oxygenation*; Melezhik, V.A., Ed.; Springer: Berlin/Heidelberg, Germany, 2013; Volume 2, pp. 39–110.
37. Kudryashov, N.M.; Udoratina, O.V.; Kalinin, A.A.; Lyalina, L.M.; Selivanova, E.A.; Grove, M.J. U-Pb (SHRIMP-RG) age of zircon from rare-metal (Li, Cs) pegmatites of the Okhmylk deposit of the Kolmozero-Voron'ya greenstone belt (northeast of the Fennoscandian shield). *J. Min. Inst.* **2022**, *255*, 448–454. [CrossRef]
38. Antonyuk, E.S. *Structural-Mineral Complexes of Granite Pegmatite Veins, Materials on the Mineralogy of the Kola Peninsula*; KFAN USSR: Apatity, Russia, 1962; pp. 134–142. (In Russian)
39. Polkanov, A.A.; Gerling, E.K. Geochronology and geological evolution of the Baltic Shield and its folded framing. *Tr. LAGED* **1961**, *12*, 101–102. (In Russian)
40. Černý, P.; Ercit, S. The classification of granitic pegmatites revisited. *Can. Mineral.* **2005**, *43*, 2005–2026. [CrossRef]
41. Müller, A.; Romer, R.L.; Pedersen, R.B. The Sveconorwegian pegmatite province—Thousands of pegmatites without parental granites. *Can. Mineral.* **2017**, *55*, 283–315. [CrossRef]
42. Webber, K.L.; Simmons, W.B.; Falster, A.U.; Hanson, S.L. Anatectic pegmatites of the Oxford County pegmatite field, Maine, USA. *Can. Mineral.* **2019**, *57*, 811–815. [CrossRef]
43. Silva, D.; Groat, L.; Martins, T.; Linnen, R. Structural controls on the origin and emplacement of lithium-bearing pegmatites. *Can. J. Mineral. Petrol.* **2023**, *61*, 2300045. [CrossRef] [PubMed]
44. Zhao, Z.; Yang, X.; Lu, S.; Lu, Y.; Sun, C.; Chen, S.; Chen, S.S.; Zhang, Z.Z.; Bute, S.I.; Zhao, L.L. Genesis of Late Cretaceous granite and its related Nb-Ta-W mineralization in Shangbao. Nanling Range: Insights from geochemistry of whole-rock and Nb-Ta minerals. *Ore Geol. Rev.* **2021**, *131*, 103975. [CrossRef]
45. Alfonso, P.; Hamid, S.; Garcia-Valles, M.; Llorens, T.; López Moro, F.; Tomasa, O.; Calvo, D.; Guasch, E.; Anticoi, H.; Oliva, J.; et al. Textural and mineral-chemistry constraints on columbite-group minerals in the Penouta deposit: Evidence from magmatic and fluid-related processes. *Mineral. Mag.* **2018**, *82* (Suppl. S1), 199–222. [CrossRef]
46. Tindle, A.G.; Breaks, F.W. Columbite-tantalite mineral chemistry from rare-element granitic pegmatites: Separation Lakeh area, NW Ontario. *Canada. Mineral. Petrol.* **2000**, *70*, 165–198. [CrossRef]
47. Černý, P. The Tanco rare-element pegmatite deposit, Manitoba: Regional context, internal anatomy, and global comparisons. In *Rare-Element Geochemistry and Mineral Deposits*; GAC Short Course Notes; Linnen, R.L., Samson, I.M., Eds.; Geological Association of Canada: St. John's, NL, Canada, 2005; Volume 17, pp. 127–158.
48. Chudík, P.; Uher, P.; Gadas, P.; Škoda, R.; Pršek, J. Niobium-tantalum oxide minerals in the Jezuitské Lesy granitic pegmatite, Bratislava Massif, Slovakia: Ta to Nb and Fe to Mn evolutionary trends in a narrow Be, Cs-rich and Li, B-poor dike. *Mineral. Petrol.* **2011**, *102*, 15–27. [CrossRef]
49. Lahti, S.I. Zoning in columbite-tantalite crystals from the granitic pegmatites of the Eräjärvi area, southern Finland. *Geochim. Cosmochim. Acta* **1987**, *51*, 509–517. [CrossRef]
50. Van Lichtervelde, M.; Linnen, R.L.; Salvi, S.; Beziat, D. The role of metagabbro rafts on tantalum mineralization in the Tanco granitic pegmatite, Manitoba. *Can. Mineral.* **2006**, *44*, 625–644. [CrossRef]
51. Van Lichtervelde, M.; Holtz, F.; Melcher, F. The effect of disequilibrium crystallization on Nb-Ta fractionation: Contraints from crystallization experiments of tantalite-tapiolite. *Am. Mineral.* **2018**, *103*, 1401–1416. [CrossRef]
52. London, D. Ore-forming processes within granitic pegmatites. *Ore Geol. Rev.* **2018**, *101*, 349–383. [CrossRef]

53. Jahns, R.H.; Burnham, C.W. Experimental studies of pegmatite genesis: I, A model for the derivation and crystallization of granitic pegmatites. *Econ. Geol.* **1969**, *64*, 843–864. [CrossRef]
54. Novák, M.; Černý, P.; Uher, P. Extreme variation and apparent reversal of Nb-Ta fractionaction in columbite-group minerals from the Scheibengraben beryl-columbite granitic pegmatite, Maršíkov, Czech Republic. *Eur. J. Mineral.* **2003**, *15*, 565–574. [CrossRef]
55. Galliski, M.A.; Márquez-Zavalia, M.F.; Černý, P.; Martínez, V.A.; Capman, R. The Ta-Nb-Sn-Ti oxide mineral paragenesis from La Viquita, a spodumene bearing rare-element granitic pegmatite, San Luis, Argentina. *Can. Mineral.* **2008**, *30*, 379–393. [CrossRef]
56. Wise, M.A.; Brown, C.D. Mineral chemistry, petrology and geochemistry of the Sebago granite–pegmatite system, southern Maine, USA. *J. Geosci.* **2010**, *55*, 3–26. [CrossRef]
57. Zhu, Z.Y.; Wang, R.C.; Che, X.D.; Zhu, J.C.; Wei, X.L.; Huang, X. Magmatic–hydrothermal rare element mineralization in the Songshugang granite (northeastern Jiangxi. China): Insights from an electron-microprobe study of Nb–Ta–Zr minerals. *Ore Geol. Rev.* **2015**, *65*, 749–760. [CrossRef]
58. Feng, Y.G.; Liang, T.; Yang, X.Q.; Zhang, Z.; Wang, Y.Q. Chemical evolution of Nb- Ta Oxides and Cassiterite in phosphorus-rich albite-spodumene pegmatites in the Kangxiwa-Dahongliutan pegmatite field, Western Kunlun Orogen, China. *Minerals* **2019**, *9*, 166. [CrossRef]
59. Duan, Z.-P.; Jiang, S.-Y.; Su, H.-M.; Zhu, X.Y.; Zou, T. Nb-Ta oxides as recorders of hydrothermal activity in the Shihuiyao Rb-Nb-Ta-(Be-Li) deposit, Inner Mongolia, NE China. *Ore Geol. Rev.* **2022**, *150*, 105149. [CrossRef]
60. Shchekina, T.I.; Gramenitskii, E.N. Geochemistry of Sc in the magmatic process: Experimental evidence. *Geochem. Int.* **2008**, *46*, 351–366. [CrossRef]
61. Von Knorring, O.; Fadipe, A. On the mineralogy and geochemistry of niobium and tantalum in some granite pegmatites and alkali granites of Africa. *Bull. Minéral.* **1981**, *104*, 496–507. [CrossRef]
62. Breiter, K.; Skoda, R.; Uher, P. Nb–Ta–Ti–W–Sn-oxide minerals as indicators of a peraluminous P- and F-rich granitic system evolution: Podlesí, Czech Republic. *Mineral. Petrol.* **2007**, *91*, 225–248. [CrossRef]
63. Linnen, R.L.; Keppler, H. Columbite solubility in granitic melts: Consequences for the enrichment and fractionation of Nb and Ta in the Earth's crust. *Contrib. Mineral. Petrol.* **1997**, *128*, 213–227. [CrossRef]
64. Fiege, A.; Kirchner, C.; Holtz, F.; Linnen, R.L.; Dziony, W. Influence of fluorine on the solubility of manganotantalite ($MnTa_2O_6$) and manganocolumbite ($MnNb_2O_6$) in granitic melts—An experimental study. *Lithos* **2011**, *122*, 165–174. [CrossRef]
65. Kaeter, D.; Barros, R.; Menuge, J.F. Metasomatic High Field Strength Element, Tin, and Base Metal Enrichment Processes in Lithium Pegmatites from Southeast Ireland. *Econ. Geol.* **2021**, *116*, 169–198. [CrossRef]
66. Zhang, D.H.; Zhang, W.H.; Xu, G.J. The ore fluid geochemistry of F-rich silicate melt-hydrous fluid system and its metallogeny-the current status and problems. *Earth Sci. Front.* **2004**, *11*, 479–490.
67. Seward, T.M.; Barnes, H.L. Metal transport by hydrothermal ore fluids. *Geochem. Hydrotherm. Ore Depos.* **1997**, *3*, 435–486.

Disclaimer/Publisher's Note: The statements, opinions and data contained in all publications are solely those of the individual author(s) and contributor(s) and not of MDPI and/or the editor(s). MDPI and/or the editor(s) disclaim responsibility for any injury to people or property resulting from any ideas, methods, instructions or products referred to in the content.